**Department of Environment Systems**
**Graduate School of Frontier Sciences**
**The University of Tokyo**

# 2016

# Master's Thesis

## Simulating urban-heat-island influenced subsurface temperature distribution considering groundwater flow in Meguro, Tokyo: A trial on 3-D model building

## (アーバンヒートアイランドが影響する地中温度分布のシミュレーションに地下水流動を加えて : 東京・目黒を現地としての三次元モデルの構築)

Submitted February 23, 2017

Supervisor: Professor TOKUNAGA Tomochika
Co-advisor: Assistant professor AICHI Masaatsu

DU Mengchan

**Abstract**

Subsurface temperature increase is observed widely around the world. One way, the warming of underground is worried for its potential negative impact to human health, e.g., by influencing the drinking water quality, while on the other hand, some view it as a potential source of shallow geothermal energy. To further discuss utilization of the shallow geothermal energy, subsurface temperature distribution simulated by a 3-D approximation of the studied strata was considered to be helpful for selecting installation spot of geothermal facilities. However, groundwater flow factor has not been considered in a 3-D simulation of subsurface temperature yet. Hence this study aims at building a 3-D model of subsurface temperature while considering groundwater flow using FEFLOW simulator. Appropriateness of the modeling approach was inspected initially, after which quality of the 3-D model built was estimated by its ability to reproduce local groundwater contour and to catch the influence of groundwater flow to subsurface temperature. Temperature distributions under scenario of urban heat island were simulated considering groundwater flow and excluding groundwater flow, respectively, which were compared to each other to inspect the influence of flow to temperature distribution. The results showed that (i) current modeling approach is reliable, that local groundwater flow can be well reproduced by a steady-state simulation of the 3-D flow-UHI joint model built, and the influence of groundwater flow to subsurface temperature can be caught by the 3-D model; (ii) groundwater flow do influence subsurface temperature distribution, hence the approach here in this study is considered helpful to improve the accuracy of mapping the heat stock of subsurface UHI. Moreover, sewage system sis better added to such simulation for a more realistic approximation of the underground thermal environment

**Table of contents**

**List of figures**

**List of tables**

# 1 Introduction

## 1.1 Subsurface temperature increase and the debate on it

Subsurface temperature increase in urban area, especially in city centers was observed globally [1, 2, 3], and this phenomenon is termed as underground urban heat island (UHI) or subsurface UHI in literature [2, 4, 5]. The temperature increase in subsurface is linked to land use[3], and besides, some researchers have noticed that underground exploitation e.g., running of underground infrastructures can lead the temperature to increase in underground space[6,7,2,8].

One way, the subsurface UHI was stated as a disturbance of human activities to the natural thermal state of the underground space [6,1], whose potential negative impact to the environment is worried. Impact of the subsurface UHI on drinking water was reported [5], and furthermore, the correlation between urban green areas and subsurface warming was investigated, aimed to provide information on coping with the warming[9].

However, on the other hand, at urban sites which are warmer in subsurface than their surrounding rural sites, an overall higher COP of heat pump facilities was observed [10]. And some researchers positively insist that the subsurface UHI can be a potential source of shallow geothermal energy [11, 7, 8].

## 1.2 Approaching anthropogenic shallow geothermal energy

This study takes the viewpoint that subsurface temperature increase is a hopeful shallow geothermal energy. For utilization of such shallow geothermal energy, a spatial distribution of subsurface temperature has been considered to be useful for selecting an installation site of geothermal facilities.

Spatial distribution of anthropogenic heat flux into the urban aquifer was simulated in two Germany cities based on temperature data [8], but without considering groundwater flow. Also, even simulation on subsurface temperature in the strata heated by subway tunnels observed the groundwater flow factor[7], the observation in a 3-D model has not been done yet. However, a 3-D

model is considered to be a better approximation of the strata than a 2-D schematic model.

Thus, considering groundwater flow in 3-D model is necessary for obtaining a precise subsurface temperature distribution to represent the real. This is because that a 3-D model can contain more information of study area than the 2-D one, e.g. elevation; and heat is very possibly transferred through advection when groundwater flow appears, which is a potential factor influencing the temperature distribution.

### 1.3 Objectives and the structure of this study

As introduced above, subsurface temperature increase is a hopeful source for shallow geothermal energy even meanwhile is a potential environment risk as the subsurface UHI. Taking the positive view and approaching the phenomenon, visualizing the spatial distribution of subsurface temperature is considered significant for enabling a direct observation of the potential heat stock initially before further discussions. In this way, facilitating the accuracy of subsurface temperature distribution map is meaningful. Hence, this study aims at adding groundwater flow factor to the 3-D simulation of urban-heat-island influenced subsurface temperature, which has been expected helpful for improving the accuracy of the temperature simulation.

The study is structured as Figure 1-1. First of all, a study area was chosen for model building (Chapter 2). Then simulation scenarios were designed (Chapter 3). Next, phenomena to be simulated were grasped theoretically, after which conceptual models of the simulation were built (Chapter 3). The conceptual models were then converted into numerical models in the further step (Chapter 4). The results of the numerical models were compared with measured data respectively to inspect the simulation quality, after which the results were discussed (Chapter 5), and finally the conclusions were given (Chapter 6).

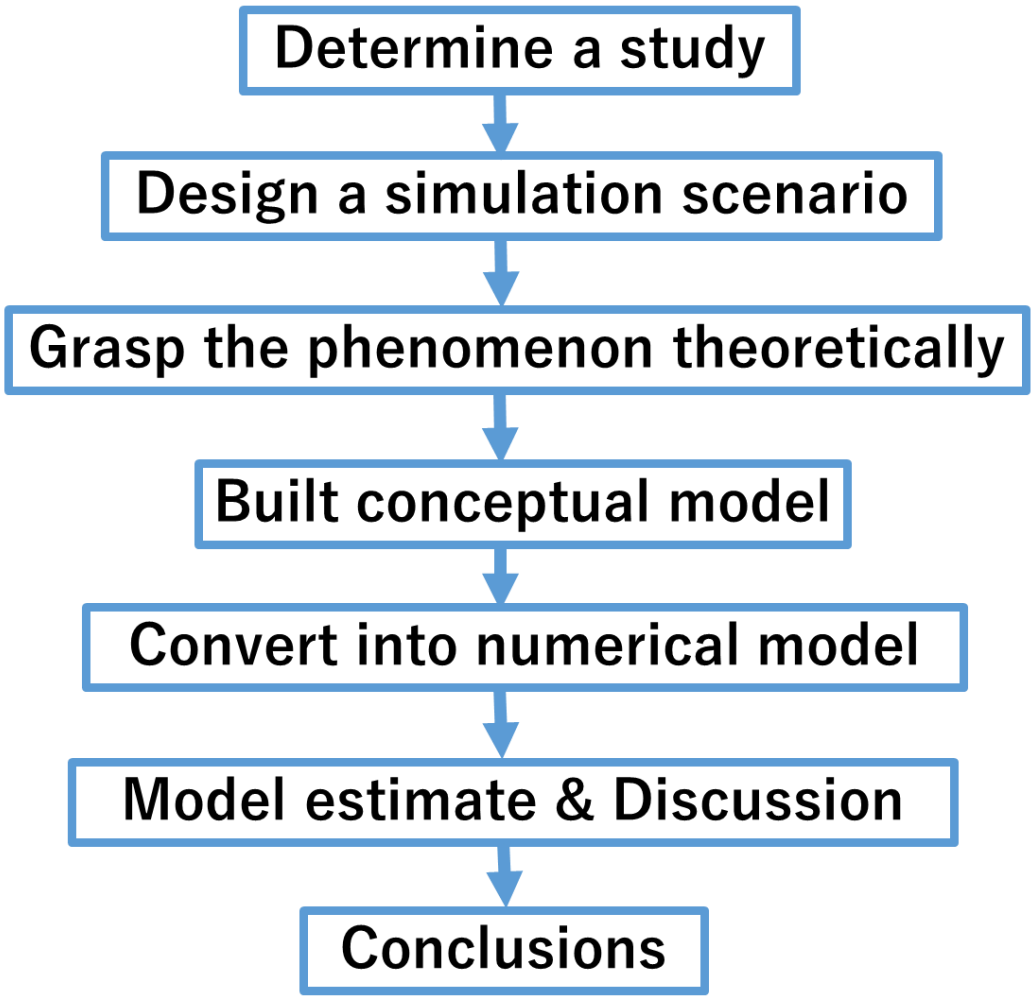


**Figure 1-1 The structure of this study**

# 2 Study area

This chapter introduces basic information of the study area in several aspects relating to the research topic.

An area near the Ohashi Junction (35.652247 N, 139.688309 E, on Google map) in Meguro Ward was chosen as the study area for 3-D model building, as an extension of a previous 2-D one [7]. The area is quite urbanized in its subsurface space, with sewage system appearing from 1960 s [12], three underground railways earliest of which was opened in 1964 [13,14], and specially, a long underground highway tunnel, the Yamate Tunnel, which is the longest highway tunnel in Japan [15]. Hence to investigate thermal influence of underground artificial constructions, this area is considered to be proper.

Shape of the study area was specified mainly by connecting ridges of local groundwater table contours, encircling the target underground constructions and the local rivers (Figure 2-1). The main parts of the target constructions were far enough from the outline of the study area (> 40 m)[7], which corresponded to the side boundary of the 3-D model. Thus it is reasonable to consider that the thermal influence of the constructions to subsurface temperature can be captured by the model made of this study area. A topographic base map was traced to portray the river and tunnels in the study area.

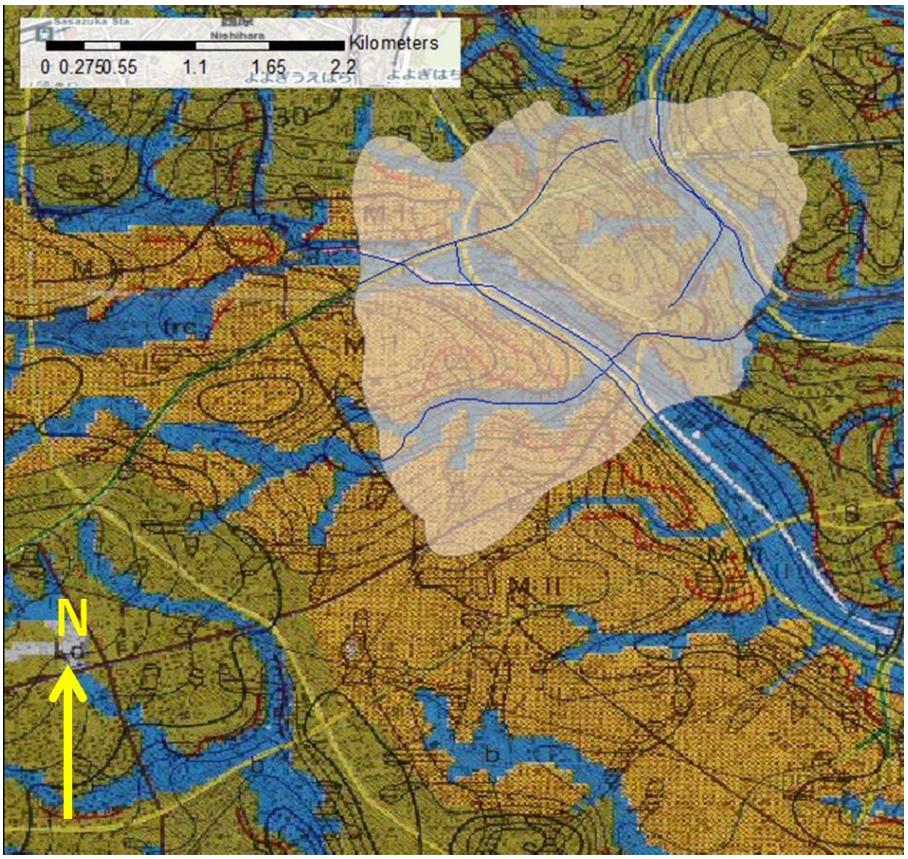


**Figure 2-1 Map of the study area (adapted from the landform classification map, Ministry of Land, Infrastructure, Transport and Tourism)**[16]

Maps were manufactured via ArcGIS software (version 10.4, ESRI), and the plane rectangular coordinate system (JGD 2000 zone 9 of the Japanese Geodetic System)[17] was used as the projection coordinate system.

## 2.1 Geology

The study area is surrounding the Meguro River and the Shibuya River, and locates in the Meguro Upland (Figure 2-2)[18]. The Meguro Upland is a part of the Musashino Upland consisting of deposits of the Musashino Gravel Layer, which originated from a geologic formation higher in elevation: the Shimosueyoshi Upland. The Shimosueyoshi Upland was eroded by the old Tama river 100~ 30 thousand years ago, making the deposition of Musashino Gravel Layer. Kanto Loam has been deposited later, overlaying on the Musashino Gravel Layer, which covers the surface of the Meguro Upland[18].

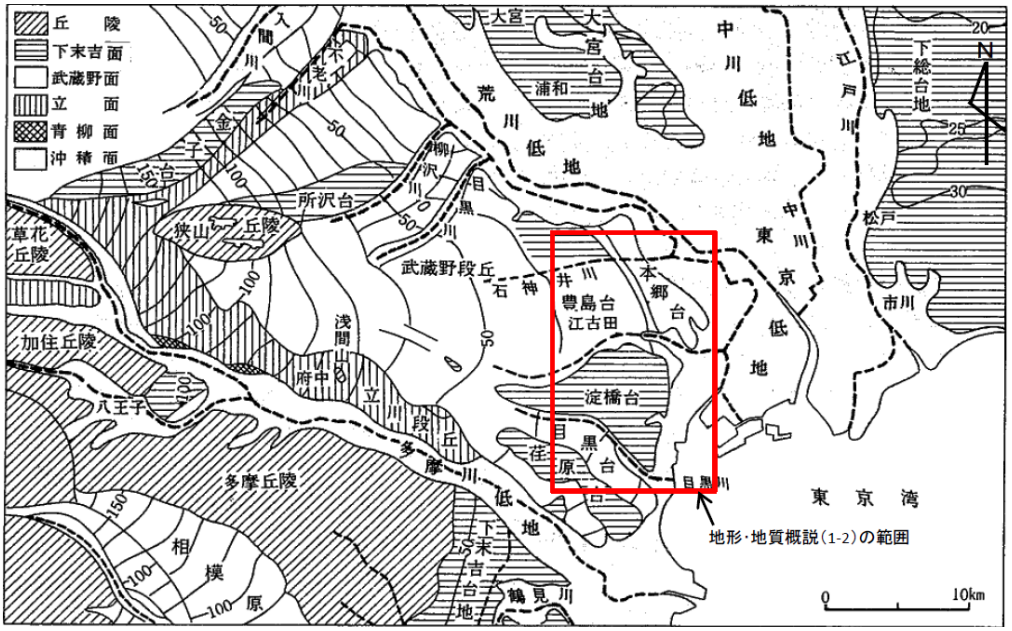


**Figure 2-2 Landform classification map in the vicinity of Musashino Upland, study area is circled by the red rectangle**[18]

## 2.2 Hydrology and hydrogeology

Around 1599 mm/year rain precipitates in the study area averagely[19], while approximately 365 mm/year of water infiltrates downwards into the underground space [20].

The Meguro River, the trunk stream in the study area, does not have a great flow[21]. Cases is the same for the neighboring river[22]. Almost all of the Kanto Loam Layer and most part of the Loamy Clay Layer have been eroded by the Meguro River, making the Musashino Gravel Layer the river bed[23]. Since the Musashino Gravel Layer is the permeable layer in the local strata through which groundwater flow (Figure 2-3, A8 is the aquifer)[24], the water level in the Meguro River is the local groundwater level. Groundwater is shallow in this area that there are many springs near the river (Figure 2-4)[25].

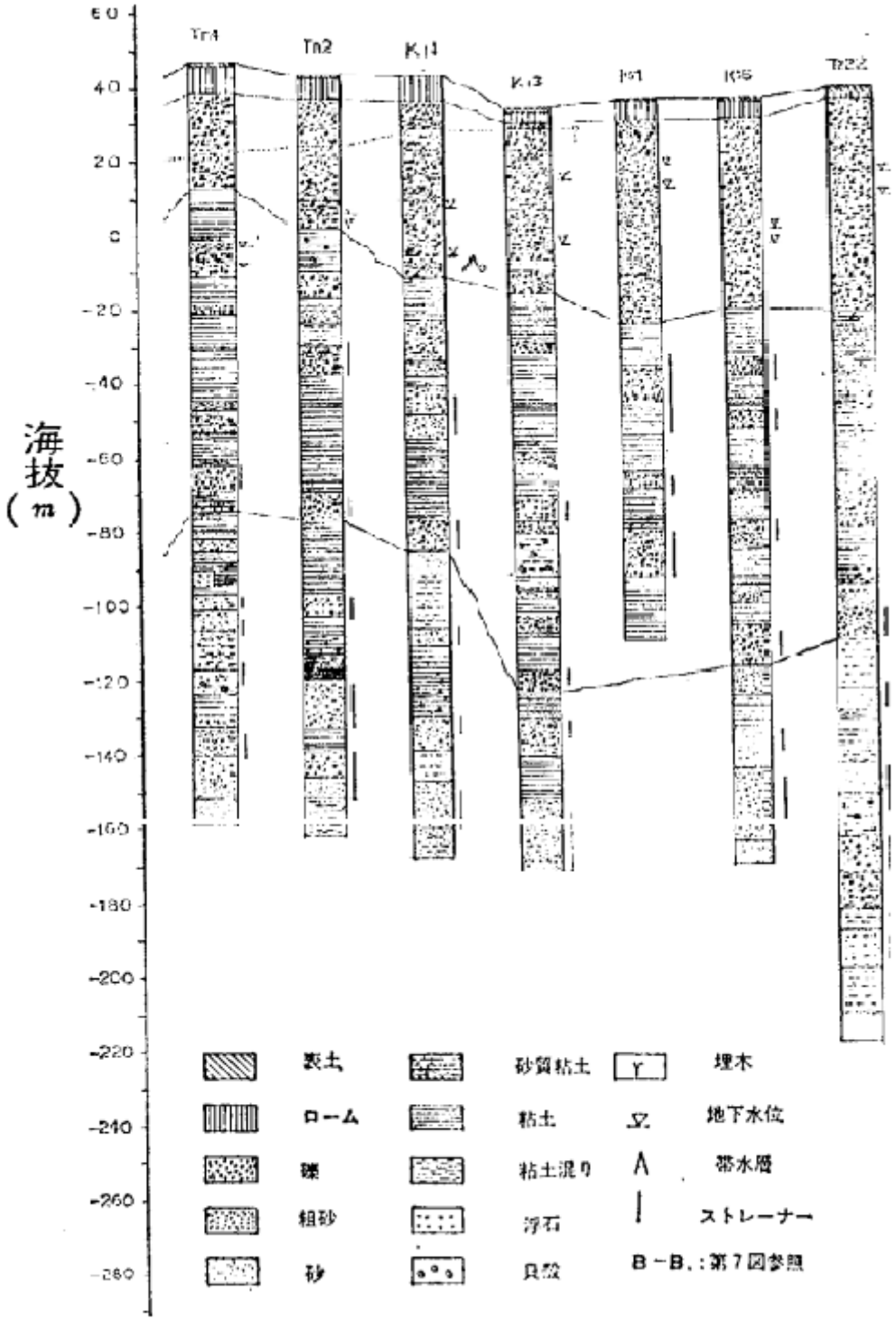


**Figure 2-3 Local groundwater level in the strata**[24]

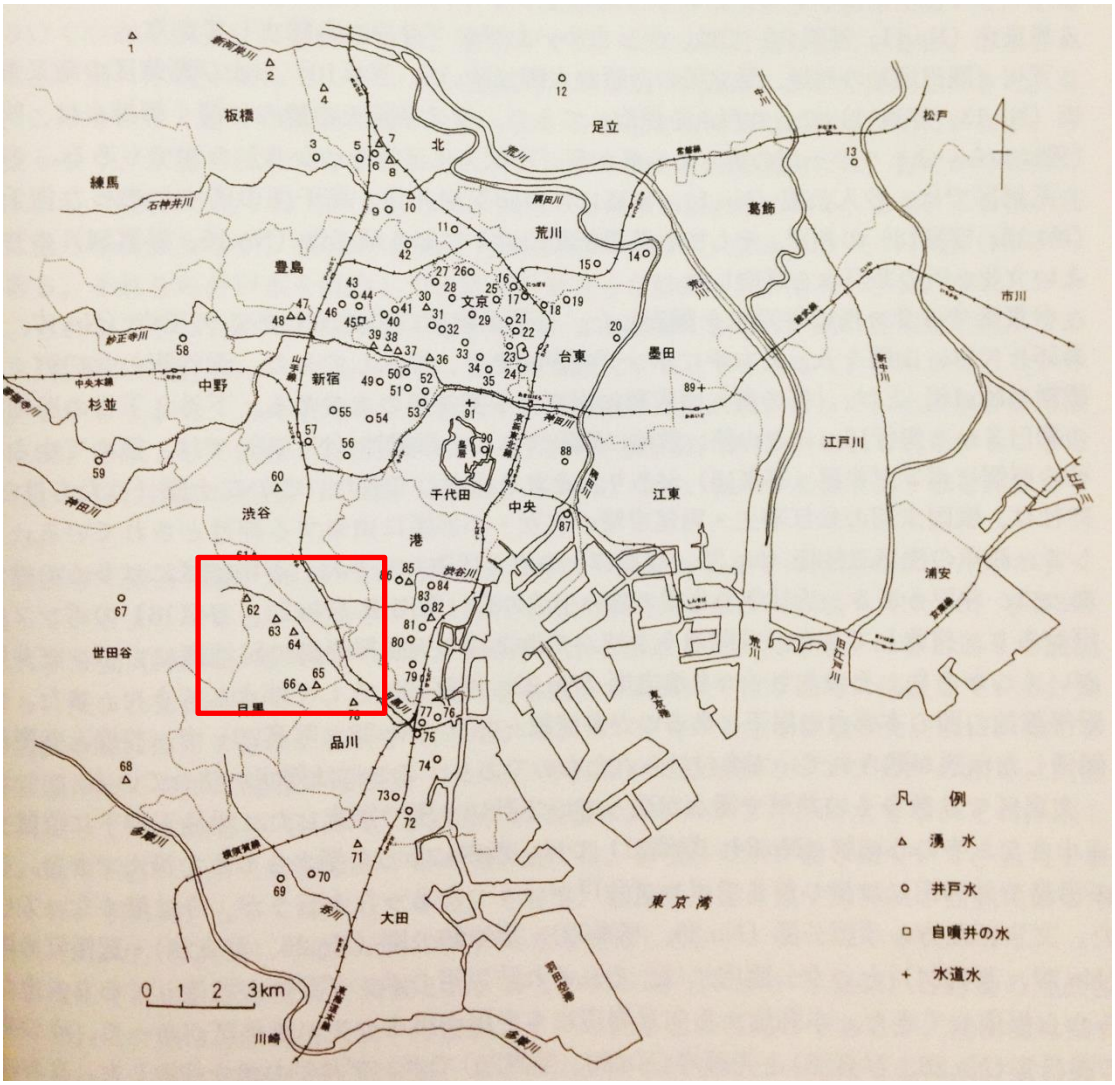


**Figure 2-4 Location of the Meguro River (marked by the red frame) and springs around it**[25]

Annual groundwater level change near the study area is not significant. The fluctuation of groundwater level is not significant along months in a year (smaller than 1 m) and this is also true for data took along years[26].

## 2.3 Land use

Solar radiation is a pathway that strata receive heat. When solar radiation reaches land surface, only a part of the radiation can be absorbed by the land, while the others are reflected. Albedo, the reflecting rate of the land surface to solar radiation, is considered to be correlated with the texture of land surface [27], which means that land use condition will influence the thermal budget of the strata, resulting in the variation of land surface temperature. Since land surface temperature will be

a direct input to the model in this study (to be introduced in 4.2.5.1), it is important to survey the land use pattern and its change in the simulation duration. Temporal changes of the land use in the study area were reported by the Geospatial Information Authority of Japan [28], as shown by Figures 2-5~ 2-7. See Figure 2-8 for the legend.

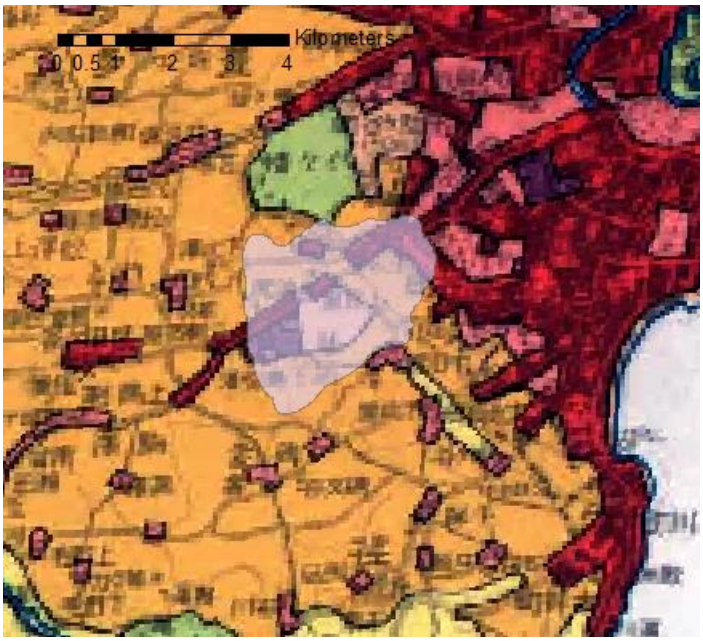


**Figure 2-5 Land use condition in vicinity of the study area, year 1914**[28]


**Figure 2-6 Land use condition in vicinity of the study area, year 1946**[28]


**Figure 2-7 Land use condition in vicinity of the study area, year 1975**[28]


**Figure 2-8 The legend of the land use map**[28]

In 1910s, the study area was almost used as a farm land, with only area near the railway urbanized. The urbanized area was extended in the mid-1940s. Until late 1970s, farm land has disappeared in the study area and its vicinity, while urbanized area was extending from the central zone of Tokyo Metropolitan to suburban villages.

## 2.4 Underground urban development

Anthropogenic heat in underground space has been assumed mainly being produced by subsurface energy consumption of human activity, namely underground space exploitation.

In the study area, the exploitation activities in underground space were summarized in Table 2-1. The Morigasaki Water Treatment Plant (now the Morigasaki Water Reclamation Center), which is the plant dealing with the sewage water released in the Meguro Ward, was opened in 1967 [12]. This is considered to be a symbol that the sewage system in the district had been somehow completed.

After the construction of sewage system, the Hibiya Line owned by the Tokyo Metro and the Denentoshi Line owned by the Tokyu Corporation were opened in year 1964 and year 1977, respectively (website of the Tokyo Metro and website of the Tokyu Corporation). Later in year 2007, an underground highway, the Yamate Tunnel was opened as a part of the Central Circular Route by the Metropolitan Expressway Company Limited [15]. Then very recently in 2013, the Tokyu Line, a subway owned by the Tokyu Corpation, was reinstalled underground for relieving the crowding situation of city function on the ground [29].

See Figure 2-9 for the location of each underground construction (sewage system not included) in the study area.

**Table 2-1 Underground exploitation in the study area**

| The Construction | Type | Opening year | Owner |
|---|---|---|---|
| Sewage system | - | 1960 s | Bureau of Sewerage, Tokyo Metropolitan Government |
| Hibiya Line | Subway | 1964 | Tokyo Metro |
| Denentoshi Line | Subway | 1977 | Tokyu Corporation |
| Tamate Tunnel | Underground highway | 2007 | Metropolitan Expressway Company Limited |
| Toyoko Line | Subway | 2013 | Tokyu Corporation |

*(*All the opening times have been referred to the official site of corresponding owner of the construction)*

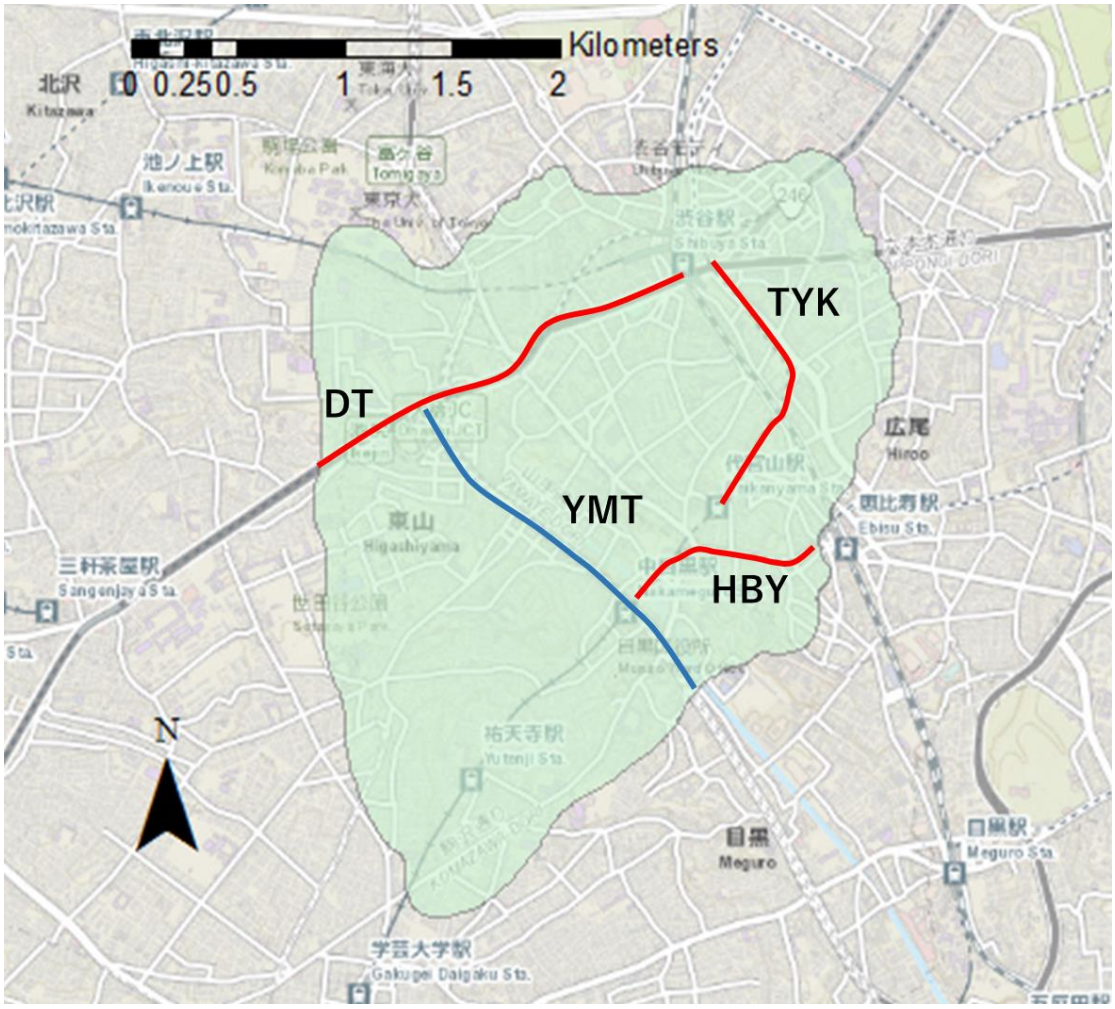


**Figure 2-9 Location of the underground constructions in the study area. Red lines represent subways (HBY: Hibiya Line, DT: Denentoshi Line, TYK: Toyoko Line), while the blue line represents the underground highway Yamate Tunnel (base map: ESRI map).**

## 2.5 Anthropogenic heat sources

Representative underground constructions (subway tunnels and an underground highway) in the study area have been focused and defined as the anthropogenic heat sources in this study. Their heating mechanisms are understood as follows: for the subway tunnel heat, air conditioning use of the train and the air conditioning use of the tunnel were mentioned in literature as heat releasing processes of the subway tunnel[30]; while for the Yamate Tunnel, outdoor air temperature, wind velocity and traffic volume inside the tunnel were reported as the main factors causing temperature increase inside the tunnel [31]. Then the released heat is transferred by advection of the air inside the tunnel from air to the tunnel well, and finally being conducted from the tunnel well to the surrounding strata.

# 3 Theory

In this chapter, simulation workflow of current study, physical theories governing the processes, conceptual understandings of the processes to be simulated are introduced.

## 3.1 Workflow of simulation

Simulation workflow in this study has been designed as Figure 3-1. At first, a 2-D cross section observing underground temperature distribution with the existence of a subway tunnel was built. Establishment of the 2-D cross section was expected to provide a modeling approach, in which groundwater flow and subsurface temperature distribution in the real can be abstracted and converted into 2-D rectangle models and further 3-D box models. Then, using this modeling approach and extending model dimension to 3-D, natural-state of subsurface temperature was obtained as a groundwater flow model combined with average land surface temperature and crustal heat flux only. The calculated groundwater contour was fixed in a UHI-influenced subsurface temperature model later to obtain the subsurface temperature distribution influenced by groundwater flow. The local groundwater flow was simulated at steady-state (see detailed explanation in 3.2.1) to obtain a generalized groundwater table contour; while for the UHI-influenced subsurface temperature simulation, transient mode was used to enable the addition of timely changing boundary conditions.

To estimate the simulations, firstly, the calculated temperature profile of the 2-D cross section was compared with a measured datum from a monitoring well to discuss the reliability of the modeling approach. Then the groundwater contour resulted from the groundwater flow simulation was compared to a measured one, while the calculated water level was inspected referring to measured groundwater level data at a well. Finally, a subsurface temperature profile calculated by the 3-D flow-UHI joint model was compared to a measured subsurface temperature profile to estimate model quality, and a comparison between the temperature distribution influenced by groundwater flow and excluding groundwater flow was conducted to see the influence of groundwater flow to subsurface temperature distribution.

Specific model settings are introduced in Chpater 4.

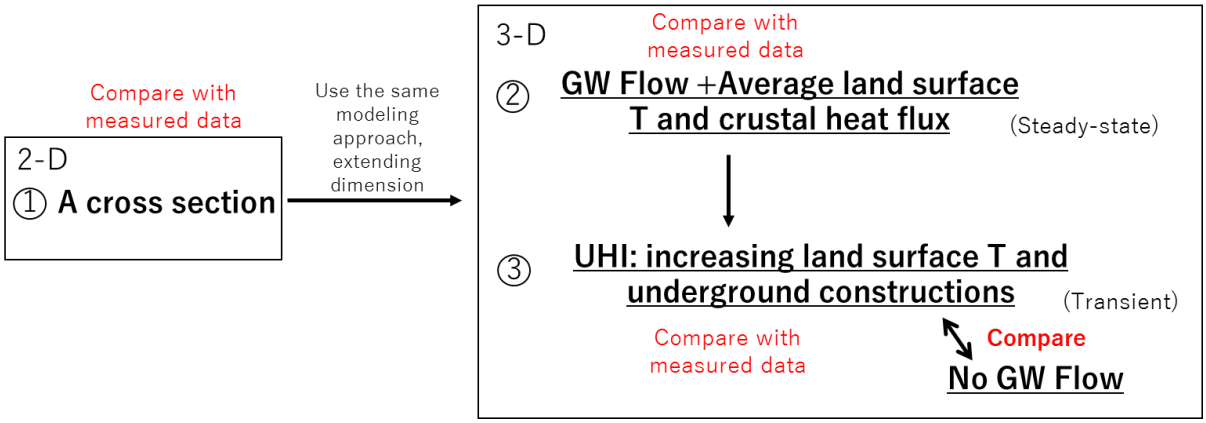


**Figure 3-1 Simulation workflow of the study**

### 3.2 Physical theories to be applied

In this section, the governing equations of groundwater flow process and heat transport process are derived respectively.

#### 3.2.1 Groundwater flow in the strata

Consider the mass balance of water in a representative elementary area (REA) in the 2-D cross section (Figure 3-2 (A)) case, and a representative elementary volume (REV) in the 3-D schematic strata (Figure 3-2 (B))[27]. Assume water density as $\rho$ (kg/m$^3$).

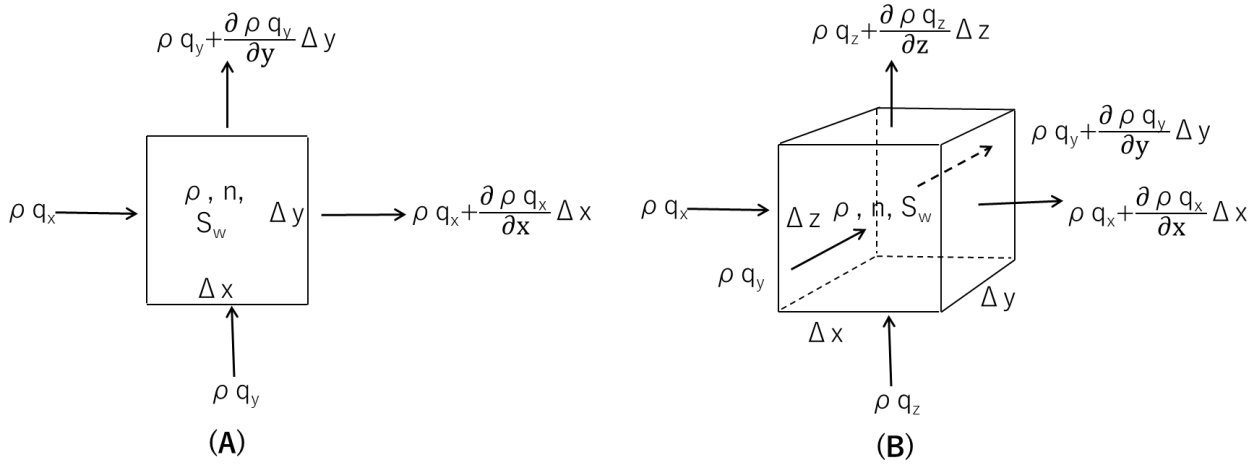


**Figure 3-2 Mass balance in (A) a REA for the 2-D cross section and (B)[27] a REV for the 3-D model**

In x direction of the 2-D case, when $\rho q_x \Delta y \Delta t$ of mass entering into the REA, there is $(\rho q_x + \frac{\partial \rho q_x}{\partial x} \Delta x) \Delta y \Delta t$ of mass draining out of the REA, where $q_x$ is the volumetric flux of water ($m^3/(m \cdot s)$). Then mass stock in x direction is

$$\rho q_x \Delta y \Delta t - (\rho q_x + \frac{\partial \rho q_x}{\partial x} \Delta x) \Delta y \Delta t = -\frac{\partial \rho q_x}{\partial x} \Delta x \Delta y \Delta t \ \text{[kg]} \quad (3\text{-}1)$$

Similarly, mass stock in y direction of the REA can be derived as

$$(\rho q_y \Delta x \Delta t + q_I) - (\rho q_y + \frac{\partial \rho q_y}{\partial y} \Delta y) \Delta x \Delta t = -\frac{\partial \rho q_y}{\partial y} \Delta x \Delta y \Delta t + q_I \ \text{[kg]} \quad (3\text{-}2)$$

Add Formula 3-1 to 3-2, the total mass stock in the REA is obtained as

$$-(\frac{\partial \rho q_x}{\partial x} + \frac{\partial \rho q_y}{\partial y}) \Delta x \Delta y \Delta t + q_I \ \text{[kg]} \quad (3\text{-}3)$$

On the other hand, the total mass stock in the REA can be derived directly from the total differential of M (Mass in the REA, kg). Since $M = n \Delta x \Delta y S_w \rho$ (n: Porosity, dimensionless; $S_w$: Saturation, %),

$$\text{Stock} = \frac{dM}{dt} \Delta t = \frac{d(n \Delta x \Delta y S_w \rho)}{dt} \Delta t = (\frac{dn}{dt} \Delta y S_w \rho + \frac{d\Delta y}{dt} n S_w \rho + \frac{dS_w}{dt} n \Delta y \rho + \frac{d\rho}{dt} n \Delta y S_w) \Delta x \Delta t \ \text{[kg]} \quad (3\text{-}4)$$

**t**: *Time period during which the mass transport has been considered, s*

To simplify the formula, convert n, Δy and ρ into correlations with the pore water pressure p

respectively in order to rewrite dn, dΔy and dρ into expressions of dp.

Firstly, derive the correlation between dΔy and dp from defining the compressibility of soil particles in vertical direction (y direction in the 2-D case) as $\alpha_s$. It can be known that

$$\frac{d\Delta y}{\Delta y}=-\alpha_s d\sigma_z \tag{3-5}$$

**$\sigma_z$**: *Effective stress on the strata*

Assume the total vertical stress as constant (Formula 3-6).

$$p+ \sigma_z= \text{constant} \tag{3-6}$$

Thus there is

$$d\sigma_z= -dp \tag{3-7}$$

Substitute $d\sigma_z$ in Formula 3-5 with Formula 3-7, here it can be obtained that

$$d\Delta y=\alpha_s \Delta y dp \tag{3-8}$$

Next, to obtain the correlation between dn and dp, consider that $\Delta S_s$, the area for soil particles in the REA should be constant (Formula 3-9).

$$\Delta S_s=(1-n)\Delta x\Delta y=\text{constant} \tag{3-9}$$

Hence, the perfect difference of $\Delta S_s$ should be zero.

$$d\Delta S_s=[(1-n)d\Delta y-\Delta y dn]\Delta x=0 \tag{3-10}$$

Thus there should have

$$(1-n)d\Delta y- \Delta y dn=0 \tag{3-11}$$

$$dn=(1-n)\frac{d\Delta y}{\Delta y}=\alpha_s(1-n)dp \tag{3-12}$$

Finally, introducing $\beta_w$, the compressibility of water to correlate dρ to dp. According to the definition of compressibility,

$$\frac{dV_w}{V_w} = -\beta_w dp \tag{3-13}$$

$\mathbf{V_w}$: *Volume of water*

Assume the mass of pore water remains constant, hence there should be

$$d(\rho V_w)= \rho dV_w+ V_w d\rho=0 \tag{3-14}$$

Derive $\frac{dV_w}{V_w}$ from Formula 3-14 and substitute it into Formula 3-13, then

$$d\rho= \beta_w \rho dp \tag{3-15}$$

Substitute Formula 3-8, 3-12 and 3-15 into Formula 3-4

$$\text{Stock} = \frac{\text{dM}}{\text{dt}}\Delta t=\rho\left[S_w(\alpha_S + n\beta_w)\frac{dp}{dt} + n\frac{dS_w}{dt}\right]\Delta x\Delta y\Delta t \tag{3-16}$$

According to the law of mass balance, Formula 3-16 should equal to Formula 3-3. Hence theoretically, groundwater flow in the strata follows the rule below.

$$-\left(\frac{\partial \rho q_x}{\partial x} + \frac{\partial \rho q_y}{\partial y}\right)\Delta x\Delta y\Delta t = \rho\left[S_w(\alpha_S + n\beta_w)\frac{dp}{dt} + n\frac{dS_w}{dt}\right]\Delta x\Delta y\Delta t \tag{3-17}$$

As introduced in 2.2, groundwater level in the study area does not change significantly along years. Hence a steady-state simulation has been thought sufficient to obtain a generalized distribution of groundwater head for the study area. Thus all time-relating terms should be turned off. Assume density of groundwater remains constant, then Formula 3-17 can be converted into

$$\frac{\partial q_x}{\partial x} + \frac{\partial q_y}{\partial y} = 0 \tag{3-18}$$

Since groundwater level is high in the area that it even springs out of the ground (see 2.2 for detailed introduction), the local strata have been assumed as fully saturated. When the hydraulic conductivity in x and y direction is written respectively as $K_x$ and $K_y$, the specific discharge q is

$$\mathbf{q}= q_x\mathbf{e_x} + q_y\mathbf{e_y} = -K_x\frac{\partial \text{h}}{\partial \text{x}}\boldsymbol{e_x} - K_y\frac{\partial \text{h}}{\partial \text{y}}\boldsymbol{e_y} = -\mathbf{K}\text{grad (h)} = -\mathbf{K}\nabla\text{h} \tag{3-19}$$

$\mathbf{e_x}$, $\mathbf{e_y}$**:** *unit vector in x direction and y direction;*

Substitute Formula 3-19 into Formula 3-18,

$$\nabla\cdot(-\mathbf{K}\nabla\text{h}) = \text{div}(-\mathbf{K}\text{gradh}) = -\left(\frac{\partial}{\partial \text{x}}\left(K_x\frac{\partial \text{h}}{\partial \text{x}}\right) + \frac{\partial}{\partial \text{y}}\left(K_y\frac{\partial \text{h}}{\partial \text{y}}\right)\right) = 0 \tag{3-20}$$

Assume the strata is isotropic, then the equation governing the groundwater flow process in the 2-D cross section is

$$K\left(\frac{\partial^2 h}{\partial x^2}+\frac{\partial^2 h}{\partial y^2}\right)=0 \tag{3-21}$$

Similarly in the 3-D schematic strata, the groundwater flow process is governed by

$$K\left(\frac{\partial^2 h}{\partial x^2}+\frac{\partial^2 h}{\partial y^2}+\frac{\partial^2 h}{\partial z^2}\right)=0 \tag{3-22}$$

### 3.2.2 Heat transport in the strata

Thermal conduction has been assumed for the heat transport in strata, while heat also carries by groundwater and transport in thermal advection. Dispersion is not considered in current study. Consider the heat budget in a REA in the 2-D cross section (Figure 3-3 (A)) and a REV in the 3-D schematic strata (Figure 3-3 (B)).

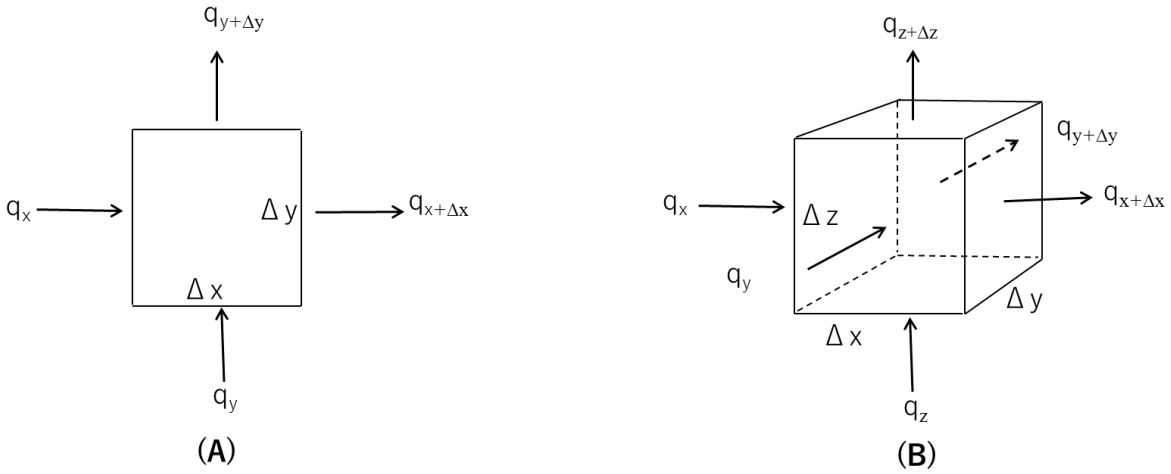


**Figure 3-3 Heat balance in (A) a REA for the 2-D cross section and (B) a REV for the 3-D model**

In the 2-D case, the volumetric flux of heat entering the REA (J/(m·s)) $q_x$ is

$$q_x=\left(-\lambda\frac{\partial T}{\partial x}+u_x\right)\Delta y|x \tag{3-23}$$

**λ**: *Thermal conductivity, W/(m • K);*

**T**: *Subsurface temperature,* ℃;

**$u_x$**: *Groundwater flow velocity in x direction, m/s*

On the other hand, the volumetric flux of heat draining out of the REA (J/(m·s)) $q_x$ should be

$$q_x=\left(-\lambda\Delta y\frac{\partial T}{\partial x}+u_x\right)\Delta y|x+\Delta x \tag{3-23}$$

Assume soil density as $\rho_s$ (kg/m$^3$) and specific heat of soil as $c_P$ (J/(kg • K)). Then, the rate of heat accumulation in the REA is

$$(\Delta x\Delta y)\rho c_P\frac{\partial T}{\partial t} \tag{3-24}$$

Assume no heat source in the REA, hence in x direction there should be

$$\left(-\lambda\frac{\partial T}{\partial x}+u_x\right)\Delta y|x-\left(-\lambda\frac{\partial T}{\partial x}+u_x\right)\Delta y|x+\Delta x=(\Delta x\Delta y)\rho c_P\frac{\partial T}{\partial t} \tag{3-25}$$

When $\Delta x\rightarrow 0$, the rate of heat accumulation in x direction is

$$\rho c_P\frac{\partial T}{\partial t}=-u_x\frac{\partial T}{\partial x}+\lambda\frac{\partial^2 T}{\partial x^2} \tag{3-26}$$

Thus for the whole REA, the rate of heat accumulation is

$$\rho c_P\frac{\partial T}{\partial t}=-(u_x\frac{\partial T}{\partial x}+u_y\frac{\partial T}{\partial y})+\lambda(\frac{\partial^2 T}{\partial x^2}+\frac{\partial^2 T}{\partial y^2}) \tag{3-27}$$

Formula 3-27 turns out to be the equation governing heat transport process in the 2-D cross section.

Similarly, in the 3-D schematic strata, governing equation for the heat transport process is

$$\rho c_P\frac{\partial T}{\partial t}=-(u_x\frac{\partial T}{\partial x}+u_y\frac{\partial T}{\partial y}+u_z\frac{\partial T}{\partial z})+\lambda(\frac{\partial^2 T}{\partial x^2}+\frac{\partial^2 T}{\partial y^2}+\frac{\partial^2 T}{\partial z^2}) \tag{3-28}$$

### 3.3 Establishing conceptual models for the processes

Conceptual captures of the phenomena to be simulated in this study are summarized in this section.

### 3.3.1 A 2-D cross section for modeling approach

Initially, a subway tunnel heating its surrounding strata in a 2-D cross section discussed by a previous study[7] was remade using another simulator to obtain a modeling approach firstly. The modeling approach was expected to be able to abstract the phenomenon of groundwater flow influenced subsurface temperature distribution in the real and convert it into 2-D rectangle models and further 3-D box models. The heat transport phenomenon in the cross section was captured schematically as Figure 3-4.

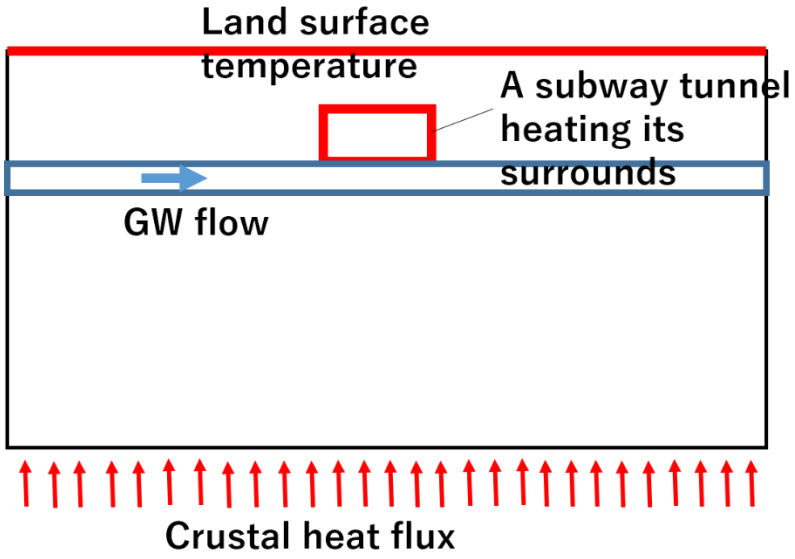


*GW: groundwater

**Figure 3-4 The schematic figure for heat transport in the 2-D cross section**

The cross section has been ideally taken as a rectangle with geologic features in it, and shape of the underground construction has been simplified. Make the side edges of the rectangle far enough from the construction, then the heat released by the construction cannot reach the side edges. Hence side edges can be treated as no heat flow boundary. The top edge of the rectangle represents the land surface into which surface temperature data were given as a boundary condition. In the bottom edge, heat flux from the crust flowing vertically into the domain has been assumed.

Groundwater flows through the stratum which is considered as the aquifer.

### 3.3.2 Extending dimension to 3-D

Use the same approach of conceptual model building, the mechanisms of local groundwater flow and the mechanisms of UHI have been captured to simulate the scenarios mentioned in 3.1 for further discussion. The 2-D rectangle has been extended into 3-D cubic boxes to represent the strata. Abstraction of the phenomena, namely conceptual models for both the groundwater flow process and the UHI process, are introduced below.

In this study, the formation of local hydraulic head distribution has been comprehended as shown in Figure 3-5: infiltration enters the model domain as potential groundwater recharge, and then the groundwater flow out of the model domain as rivers at places where the land surface elevations suddenly drop, e.g., the river bed. The river water level has been assumed to be relatively stable. The rivers flow downward the landform and finally drain out of the model domain. As mentioned in 2.2, flow in the Meguro River is very small. So for convenience of model calculation, here it has been assumed that the river receives water mainly from precipitation instead of their upstream, and in this way, side boundary of the model has been set as no groundwater flow.

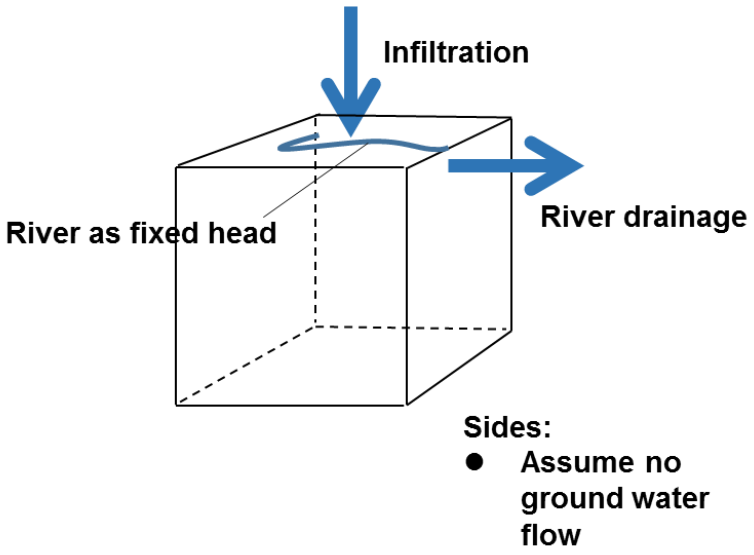


**Figure 3-5 Abstraction of local groundwater flow**

To add heat-related factors to the aforementioned groundwater flow system, measured land surface temperature has been inspected. Increasing trend of subsurface temperature has been

observed by Miura[32] (Figure 3-6). According to Azuma[33], temperature difference between air and subsurface space whose depth is less than 3 m is smaller than 0.5 ℃ in most of his study area. By this way, shallow subsurface temperature can be viewed as an approximation of the land surface temperature before 1950 s. Assume this is still true for shallow subsurface temperature and land surface temperature after 1950 s. Then approximately set the starting time of UHI as year 1945 by watching Figure 3-6, the land surface temperature can be abstracted as Figure 3-7, divided into a constant part and a yearly increasing part, representing the scenario before and after the start of subsurface UHI respectively.

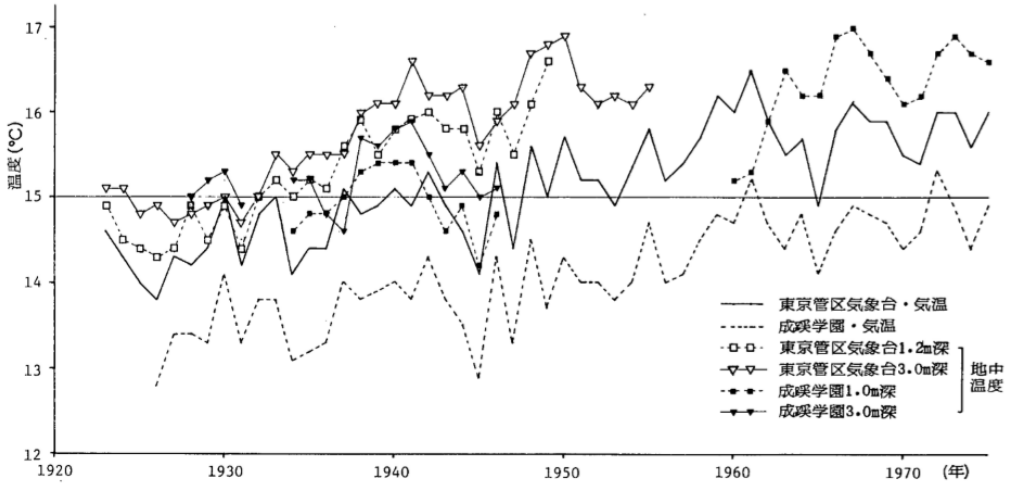


**Figure 3-6 Yearly change (1923~1975) of air and subsurface temperature observed by Miura[32]**

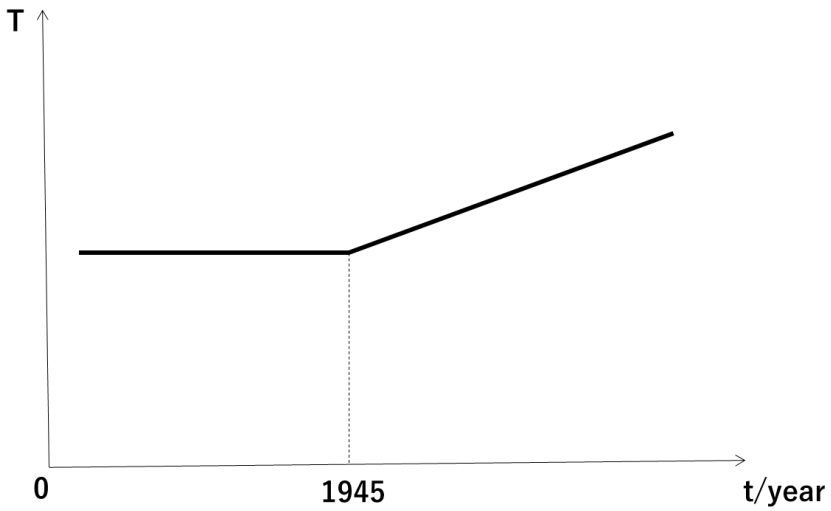


**Figure 3-7 Abstraction of land surface temperature**

Then the natural state of underground thermal environment can be schematically described as Figure 3-8. Before any artificial constructions appear, the strata were only receiving heat from solar radiation at land surface and crustal heating from the bottom, without lateral heat fluxes (assume heat fluxes induced by land surface temperature and the crust flow vertically). Hence there is no heat flux at the side boundaries. The subsurface temperature distribution was thought to be relatively stable along years in this stage.

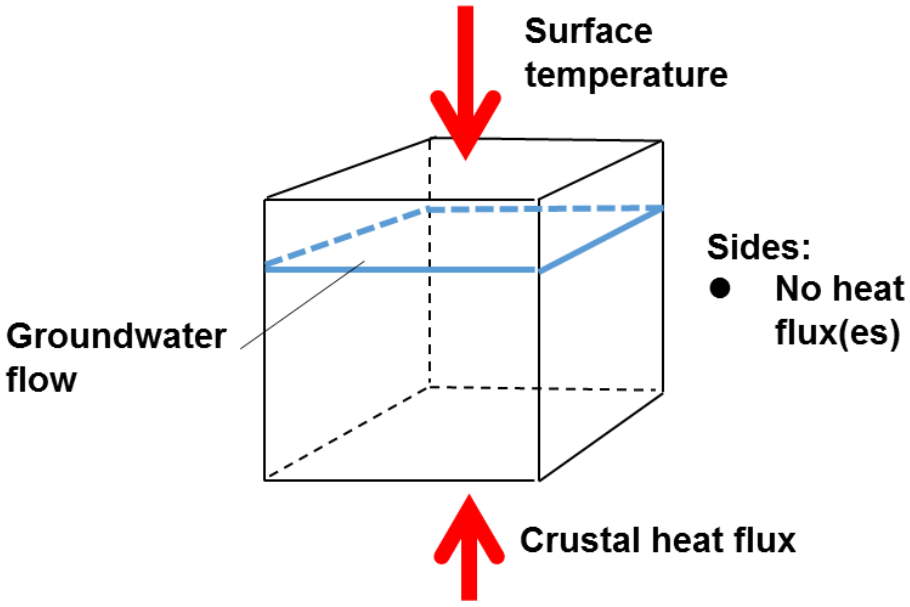


**Figure 3-8 Natural state of underground thermal environment**

After the UHI began, the land surface temperature has been assumed to increase like the trend shown in Figure 3-7 after year 1945, and artificial underground constructions heating their surroundings appear, which were added to the natural-state strata as inner heat sources (Figure 3-9).

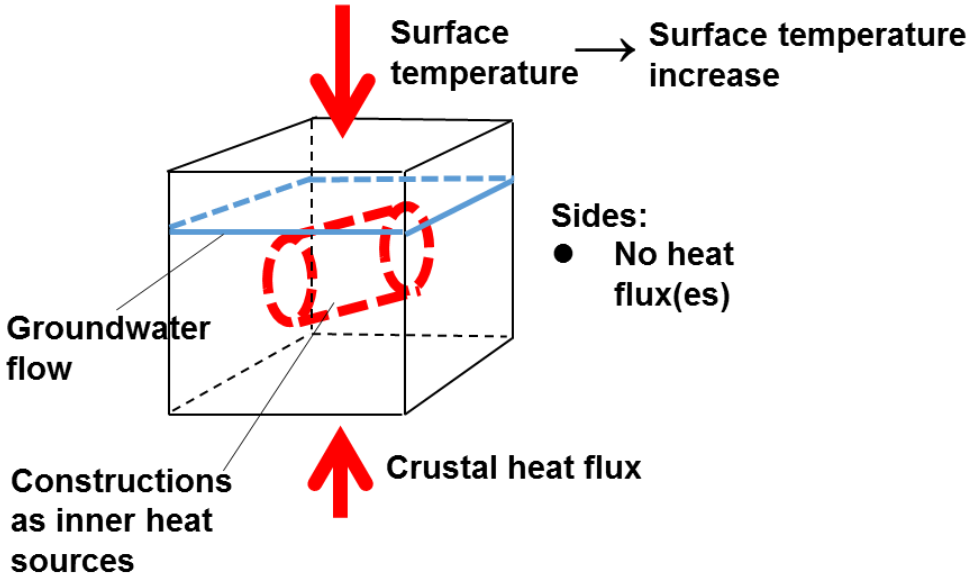


**Figure 3-9 The underground thermal environment after occurrence of UHI**

Conceptual models of phenomena introduced above were interpreted into numerical models on the next step. Finite element heat and groundwater flow modeling software FEFLOW (version 7, DHI), are used as the simulator in this study.

# 4 Model settings

In this part, specific settings including geometries, strata properties, simulation time, initial and boundary conditions of the 2-D model are introduced firstly. Then for the 3-D model, besides model geometries, strata properties and simulation time, how the groundwater flow factor being controlled is further introduced.

## 4.1 The 2-D model

A 2-D cross section with the tunnel of Tokyu Denentoshi Line in it has been repeated at the first step following a previous study conducted by Fujii[7] to obtain a modeling approach, which is expected to be able to abstract the subsurface temperature distribution and groundwater flow schematically as 2-D rectangle models then as 3-D cubic box models further. Location of the cross section is shown in Figure 4-1. Local groundwater flow direction was obtained by observing the contour of a landform classification map [16] and has been marked in Figure 4-1. Model settings were obtained referring to the previous study [7].

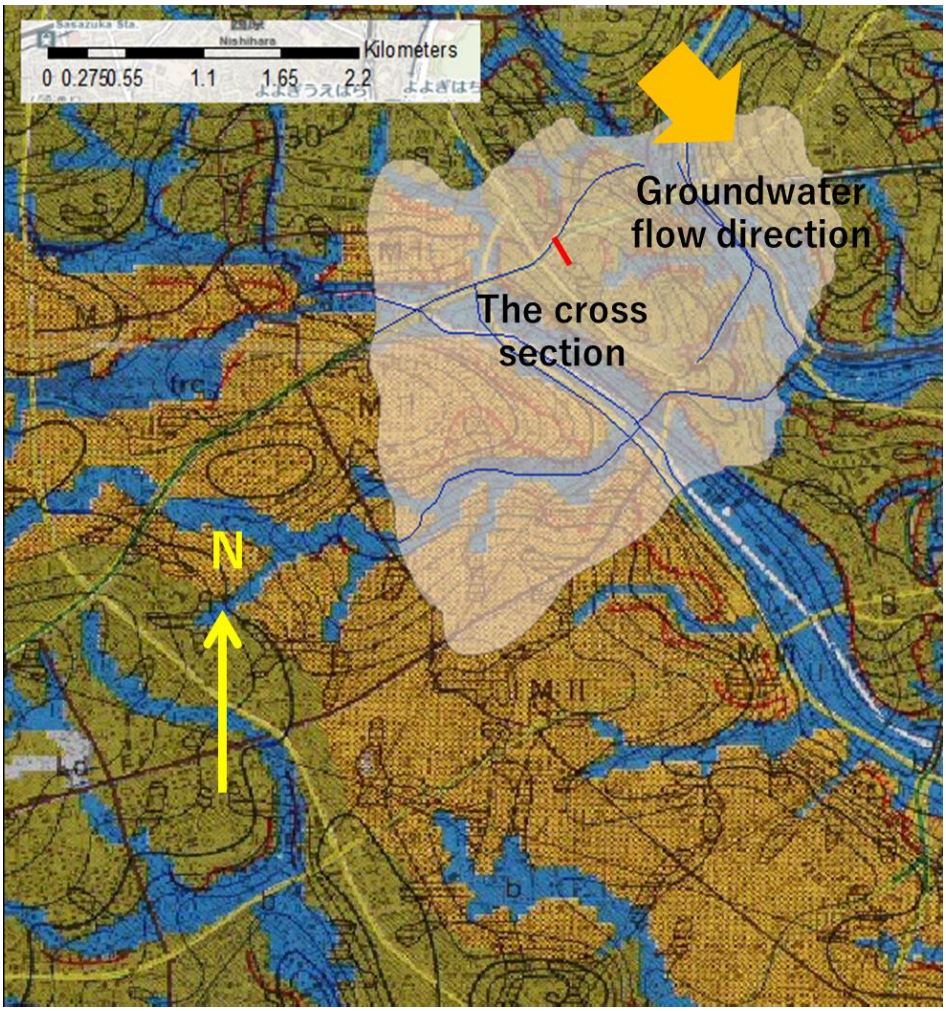


**Figure 4-1 Location of the cross section in the study area and local groundwater flow direction (source of the base map: Ministry of Land, Infrastructure, Transport and Tourism; to facilitate the easiness for spotting the cross section, the cross section has been enlarged manually. See Figure 4-4 for the real size)**[16]

### 4.1.1 Geologic layering

Geologic layering of the 2-D cross section was generally decided based on the previous study[7]. The textures of layers have been adjusted finely after inspecting a geologic cross section near the spot (Figure 4-2; see Figure 4-3 for the legend). Settings of the geologic layering, location of the aquifer, shape of the tunnel and its location in the strata are shown as Figure 4-4.

The third geologic layer in the strata- the Musashino Gravel Layer, is the aquifer through which groundwater flows. Assume groundwater flows horizontally in current schematic cross section.

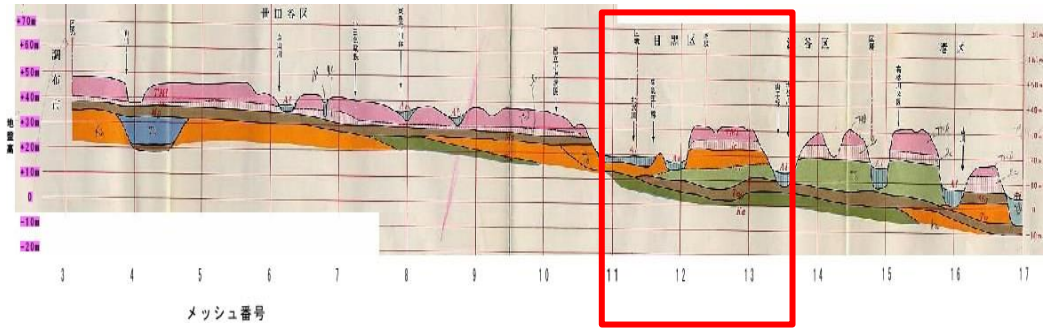


**Figure 4-2 The geologic cross section near the spot (from website of the Bureau of Construction, the Tokyo Metropolitan Government, the No. 17 cross section)[23]**

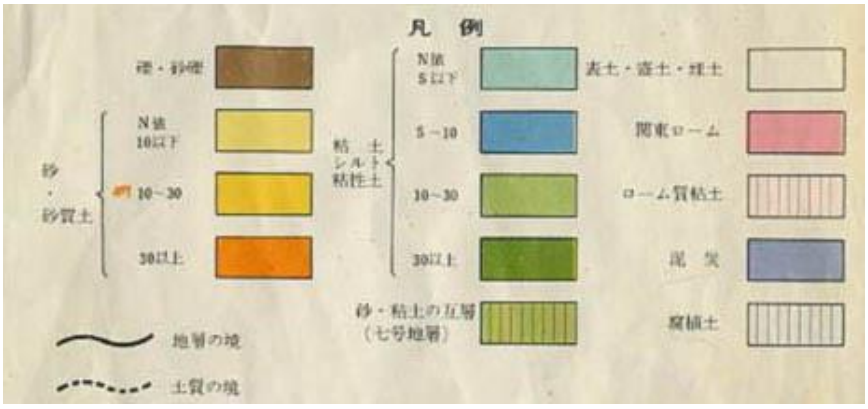


**Figure 4-3 Legend for the geologic cross section (from website of the Bureau of Construction, the Tokyo Metropolitan Government)[23]**

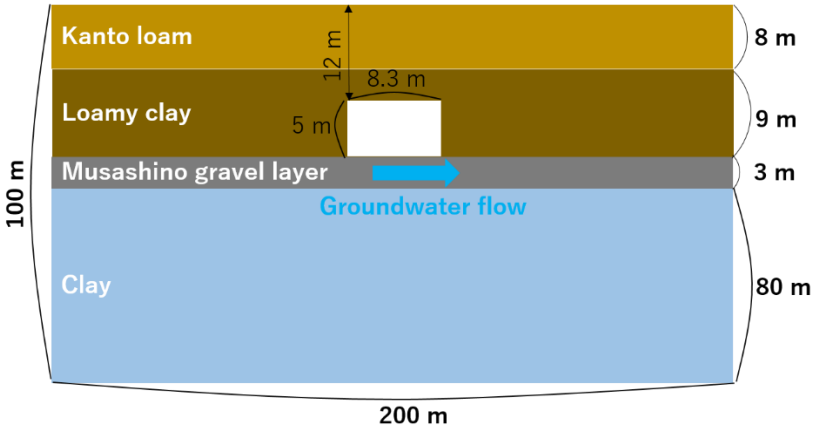


**Figure 4-4 Geologic layering of the 2-D cross section, adapted from[7]**

### 4.1.2 Physical properties of the strata and the groundwater

Hydraulic conductivities of the strata, thermal conductivities and heat capacities of both the strata and groundwater have been adopted as model parameters in this study depending on the governing

equation for groundwater flow process and heat transport process, respectively (see 3.2). Besides, strata porosities were figured out by subtracting the result of solid density dividing bulk density from 1 to meet the demand of the calculating approach of FEFLOW software. See appendix for detailed definition of each parameter.

In current 2-D model, strata-related properties were derived by adapting literature data[7], as summarized in Table 4-1; while for the properties of water, default values in the FEFLOW software have been used (see Table 4-2).

**Table 4-1 Physical properties of the strata (adapted from Fujii, 2010)[7]**

| layer | texture | hydraulic conductivity /(m/s) | thermal conductivity/ (W/mK) | specific heat/(J/m3K) | porosity |
|---|---|---|---|---|---|
| 1 | Kanto loam | 1.0E-05 | 2.6 | 3.2E+06 | 0.30 |
| 2 | Loamy clay | 5.5E-06 | 2.5 | 3.1E+06 | 0.29 |
| 3 | Musashino gravel layer | 1.0E-04 | 2.3 | 2.8E+06 | 0.18 |
| 4 | Clay | 3.0E-07 | 2.6 | 4.8E+06 | 0.31 |

**Table 4-2 Default groundwater property values in FEFLOW software**

| thermal conductivity /(W/mK) | specific heat/(J/m3K) |
|---|---|
| 0.6 | 4.2E+06 |

### 4.1.3 Temporal scenario

Current 2-D simulation was conducted following the time sequence shown in Figure 4-5. Before any artificial constructions appear in underground space, the strata were heated by the surface temperature and the crust heat flux only, and till the beginning of UHI, a balanced “natural thermal state” of the strata was thought to be reached. Hence a steady-state simulation (see “the initial condition” in 4.1.4 for detailed settings) has been conducted to obtain the natural-thermal-state subsurface temperature distribution, which was thought to be the initial condition of the model discussing thermal influence of underground human exploitation. Subsurface temperature distribution with the influence of artificial constructions was simulated

later in a transient model to describe the addition of artificial heat sources into the strata along the simulation time line. Year 1945, the time point in which UHI is considered to begin in this study was set as temporal zero point of the transient simulation. The land surface temperature increase, namely subsurface UHI (see "the boundary conditions" in 4.1.4 for the specific settings), was assumed beginning from the temporal zero point. Conditions corresponding to the subway tunnel were added to the model in its opening year (1977, the 32$^{th}$ year in the simulation duration) subsequently. The model was run continuously until 2002 (the 57$^{th}$ year in the simulation duration), right after the measurement of a subsurface temperature profile at the Meguro monitoring well. The calculated result was estimated by a comparison with the monitored data.

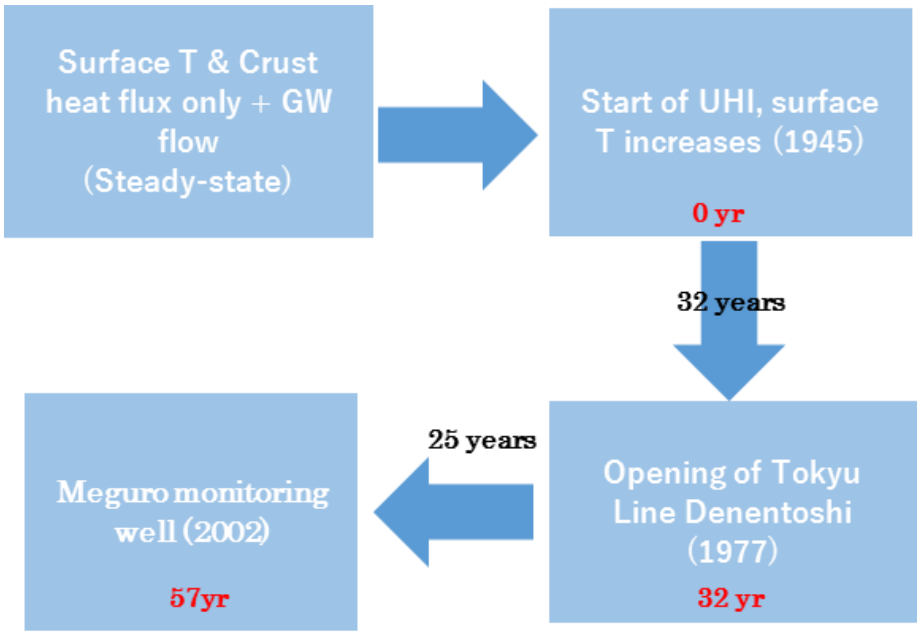


**Figure 4-5 Temporal scenario for the cross section simulation**

Groundwater flow was simulated at steady-state.

### 4.1.4 Initial and boundary conditions

The initial condition

Before human explore the underground space, there should be a "natural state" of subsurface temperature, which has been supposed to be the initial condition for the current simulation. Three

measured temperature profiles containing temperature loggings from land surface to deep underground -the FCH profile, the SHM profile and the IWT profile (for the IWT profile, data were arranged as discrete points), were summarized by Suzuki (Figure 4-6)[34]. Among observation points of these three profiles, the one of FCH is closer to the location of current 2-D cross section than the other two (Figure 4-7)[34], hence here data of FCH is discussed. To inspect whether the temperature profile monitored at FCH spot can represent the natural state of subsurface temperature, the subsurface temperature distribution excluding artificial influences have been simulated. As boundary conditions of the model, a stable land surface temperature (15 ℃, an average subsurface temperature before UHI provided by Miura[32] (see Figure 3-6), used as an approximation of the land surface temperature here) and a stable crustal heat flux (0.03 W/m$^2$ (0.76 HFU))[34] have been given. The result matched well with monitored geothermal gradient, see Figure 4-8.

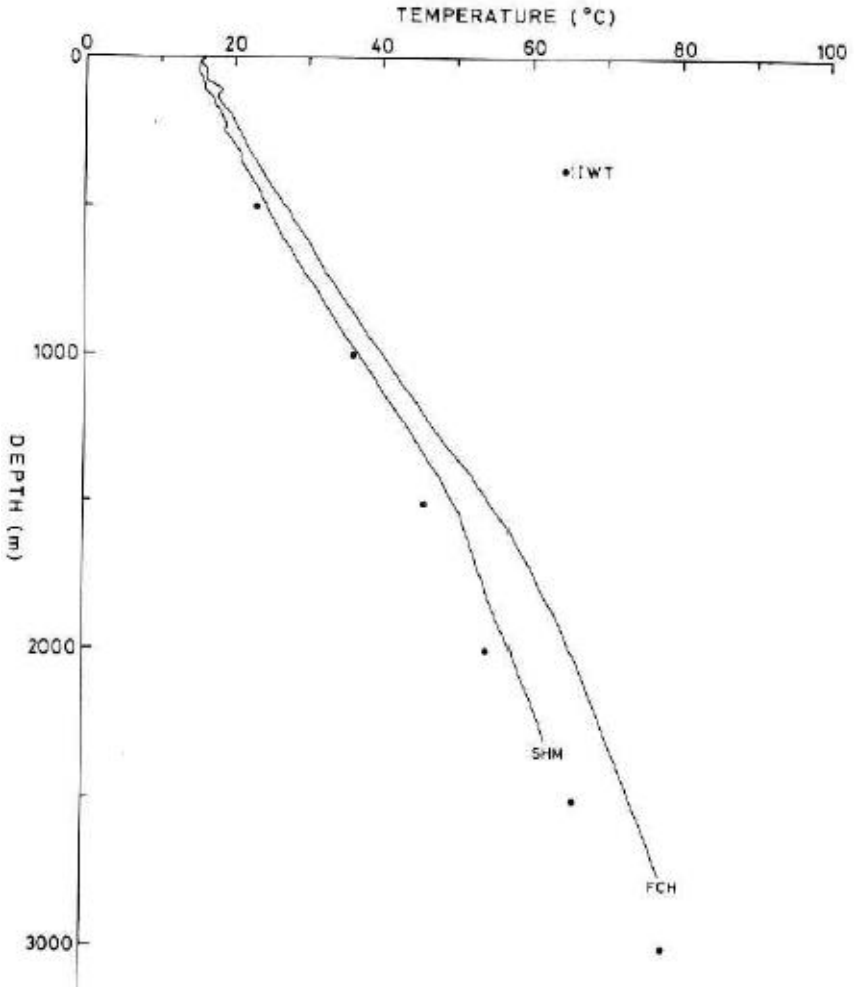


**Figure 4-6 Monitored temperature profiles at deep underground**[34]

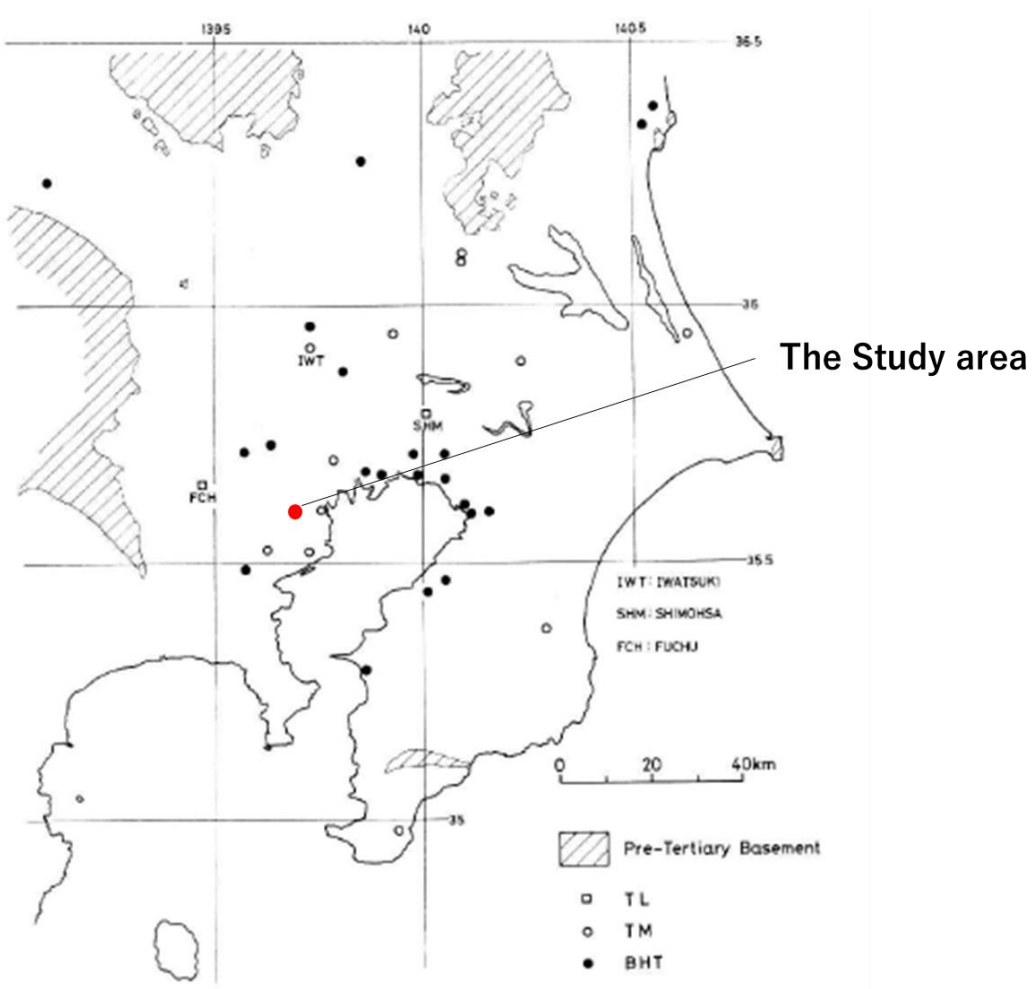


**Figure 4-7 The lcation map of the observation points for measured subsurface temperature profile (adapted from Suzuki, 1985)**[34]

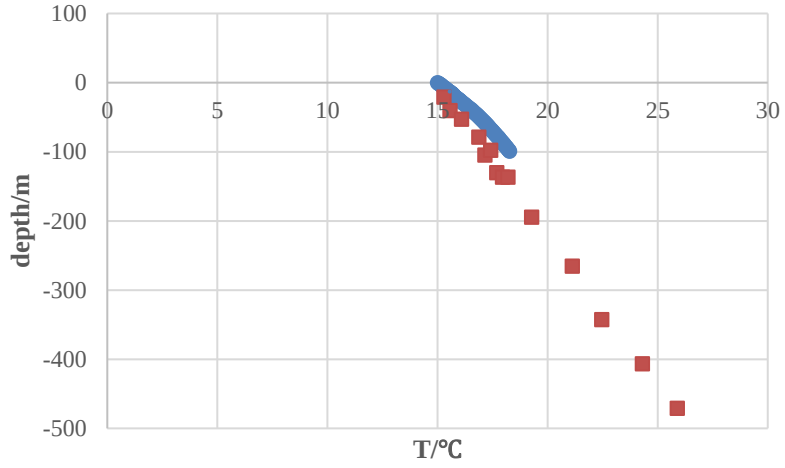


**Figure 4-8 Comparison of the calculated (blue) and monitored (red, digitized by Engauge Digitizer, version 4.1) subsurface temperature profile. In depth down to -100 m, the monitored temperature profile approximately obeys to T=15+0.015z, which was well reproduced by the simulation (source of measured data: Suzuki, 1985)**[34]

Hence the monitored temperature profile of FCH spot was given as the initial condition in the 2-D simulation.

The boundary conditions

As described in the conceptual model in 3.3.1, land surface temperature, crustal heat flux, subway tunnel temperature, and groundwater flow are given as boundary conditions to portray artificial-construction-influenced temperature distribution in the cross section. Here in this part, aforementioned boundary conditions are introduced respectively.

● The land surface temperature and crustal heat flux

Land surface temperature was based on Formula 4-1[27]. To describe the influence of UHI, a temperature increasing rate was added to the formula, which was introduced in details later in this part.

$$T(0,t)=T_0+A_0 \sin\left(\frac{2\pi t}{\tau}-\emptyset\right) \quad (4\text{-}1)$$

***$T_0$**: Average land surface temperature, ℃;*

***$A_0$**: The amplitude of land surface temperature, ℃;*

***$\tau$**: The period of land surface temperature, year;*

*∅: Phase constant, year*

In current 2-D simulation, average land surface temperature without UHI was set as 15.5 ℃, read from Figure 3-6[32]. Amplitude of asphalt surface was reported by Genchi and his colleagues from a monitor for asphalt land surface temperature at Kyoka Primary School, Chuo Ward of Tokyo[35]. Since the cross section is surrounded by highways (Figure 4-9)[36], data of asphalt was thought to be representative for the cross section. Hence, aforementioned amplitude of asphalt surface (15 ℃) was given to the formula. The period of land surface temperature and the phase constant has been set as 1 year and 0 year, respectively.


**Figure 4-9 Land surface condition near the simulated cross section (captured from Google Map)**[36]

As introduced in 3.3.2, UHI has been set to occur in year 1945. Hence to describe the influence of UHI to land surface temperature, an increasing rate of surface temperature was added to Formula 4-1. This increasing rate was quantitatively identify surface temperature increase caused by UHI, and has been derived by the following procedure. While average surface temperature before the UHI (1945) was assumed as 15 ℃, 20 ℃ of average surface temperature was observed in year 1997 (at Kyoka Primary School, Chuo Ward)[35], indicating that the land surface temperature increased 5 ℃ in 25 years. Thus for a year after the beginning of UHI (assume the

year as t), increase in surface temperature comparing to the no-urban-heat-island average temperature can be expressed as 5/52t. Adding 5/52t to Formula 4-1, then land surface temperature boundary condition in the 2-D simulation can be written as

$$T(0,t)=15℃+15\sin\left(\frac{2\pi t}{1\ \text{year}}\right)+\frac{5}{52}t \qquad (4\text{-}2)$$

For the crustal heat flux boundary, crustal heat fluxes in Knato Plain calculated by Suzuki have been referred (Figure 4-10)[34]. Here in this study, 0.03 W/m$^2$ (0.76 HFU), the data taken at the spot nearest to the studied cross section was given to the model.

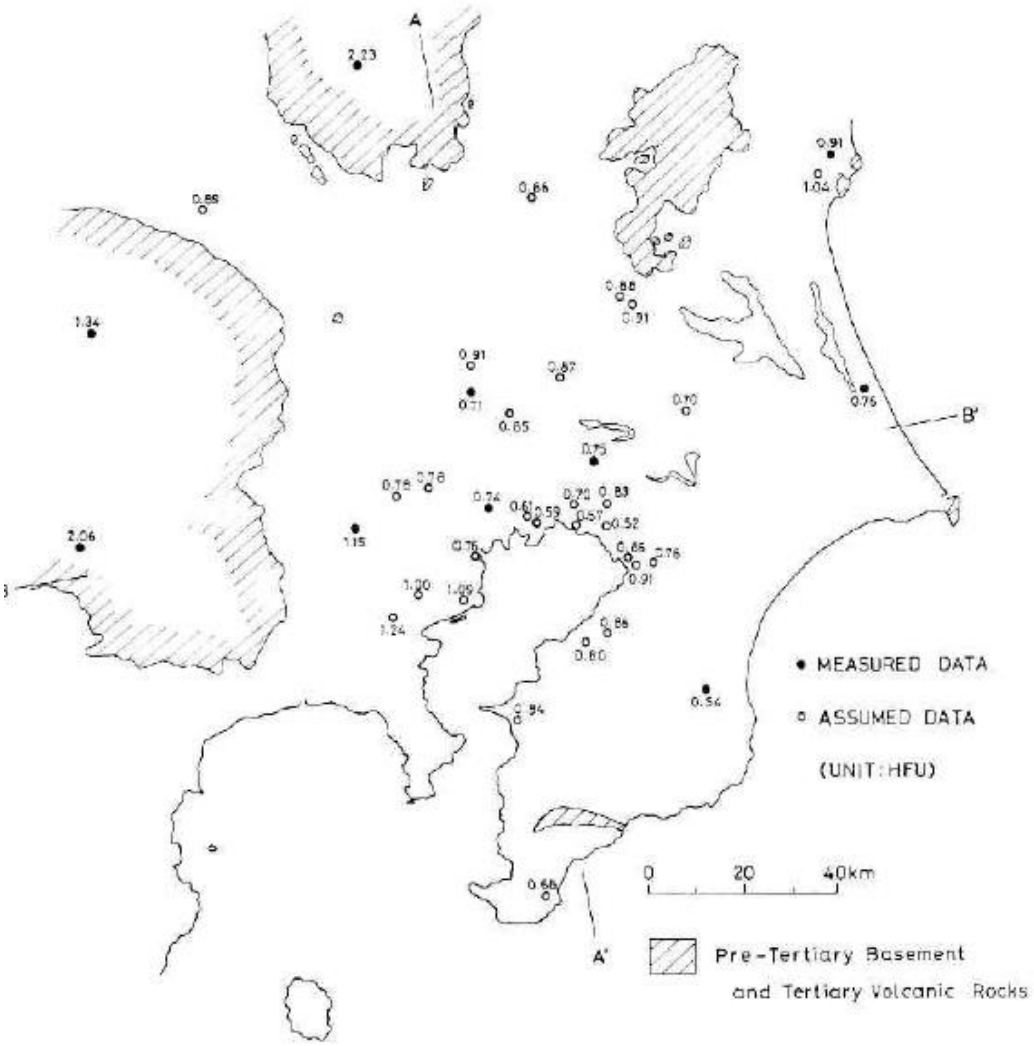


**Figure 4-10 Crustal heat fluxes in Knato Plain calculated by Suzuki**[34]

● The subway tunnel temperature

Thermal influence of the subway line has been captured as the temperature of tunnel walls heating its surrounding strata. Temperatures at the surface of concrete subway tunnels were measured in a section of Tokyo Metro Hanzomon Line from Otebori ventilating tower to Tokiwabashi ventilating tower, sandwiching Otemachi Station[37]. The monitor result was reported as a monthly changing temperature record (Table 4-3)[37], which was adapted to all the years during the simulation time.

**Table 4-3 Monthly temperature change of subway tunnel well surface, adapted from Takeda**[37]

| Month | Jan | Feb | Mar | Apr | May | Jun | Jul | Aug | Sep | Oct | Nov | Dec |
|---|---|---|---|---|---|---|---|---|---|---|---|---|
| T/℃ | 22.7 | 22.2 | 21.3 | 23.5 | 23.9 | 25.8 | 27.8 | 28.0 | 27.9 | 26.0 | 26.1 | 22.8 |

● The groundwater flow

A Darcy flow of $2.8*10^{-6}$ m/s for the local groundwater flow has been obtained by reading a landform classification map[16], and was given as a constant flow in the aquifer.

### 4.2 The 3-D model

Following the modeling approach obtained at the 2-D stage, the model dimension has been extended to 3-D (see 3.3 for conceptual details). Specific settings for the 3-D model are introduced in this section.

#### 4.2.1 Geologic layering

A rough generalized geologic layering of the 3-D model was decided by inspecting and comparing several geologic cross sections inside the study area. Information of geologic cross sections is available from the website of the Bureau of Construction, Tokyo Metropolitan Government[23].

Locating the study area into administrative division of Tokyo (Figure 4-11) to spot corresponding geologic cross section (see Figure 4-12 for the location of geologic cross sections),

it has been found that geologic cross section No. 16, 17, 18, and 19 (Figures 4-13~4-16, see Figure 4-3 for legend) are crossing through the study area. Referring to the stratigraphy of Tokyo[38], the sand stratum and the gravel stratum have been combined into one as the Musashino gravel formation. The geologic layering of the study area can be simplified as Figure 4-17. Assume strata in the study area as homogeneous and isotropic.

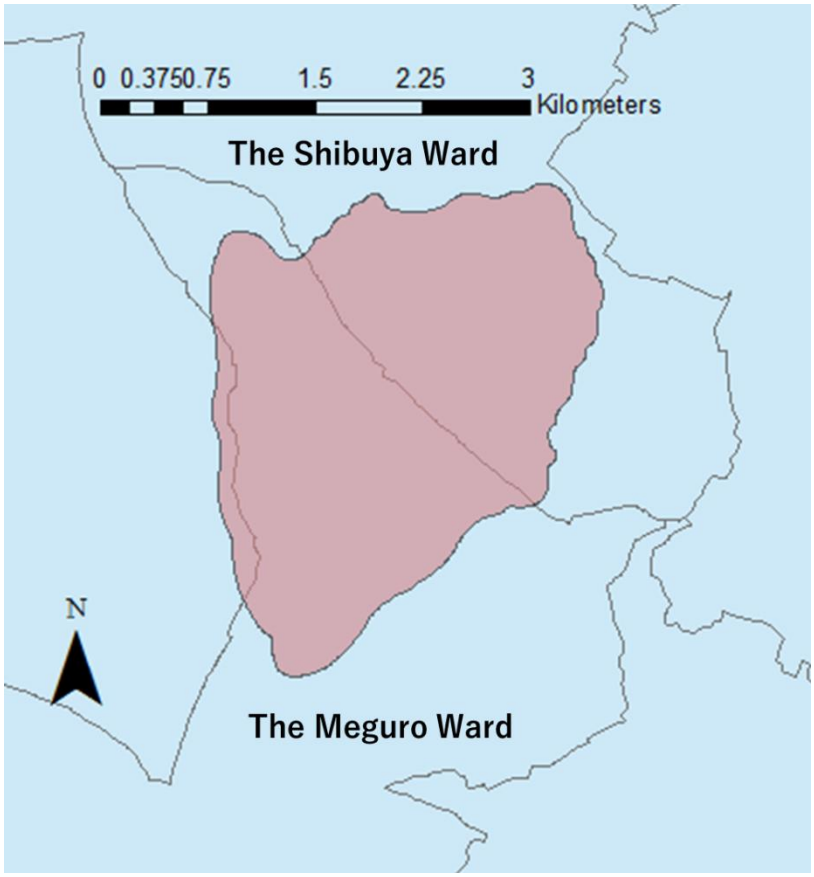


**Figure 4-11 Location of the study area in administrative division of Tokyo (base map: adapted from download center of the Geospatial Information Authority of Japan)**[39]

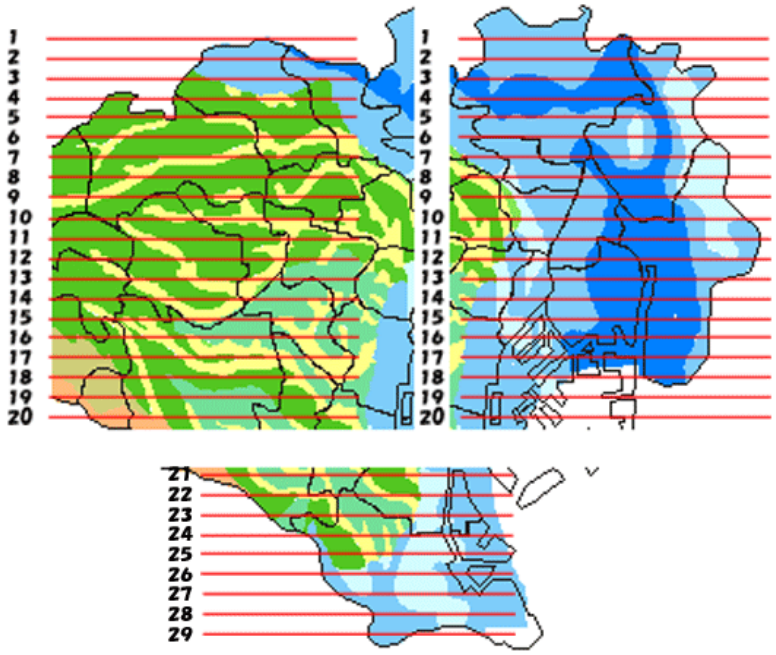


**Figure 4-12 Location of geologic cross sections (from website of the Bureau of Construction, Tokyo Metropolitan Government)[23]**

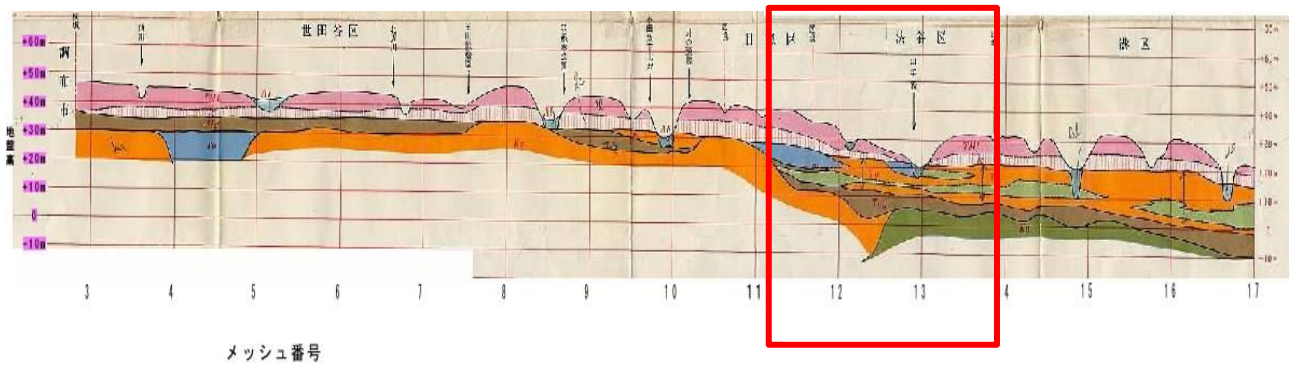


**Figure 4-13 Geologic cross section No. 16 (the left one in Figure 4-12, from website of the Bureau of Construction, Tokyo Metropolitan Government)[23]**

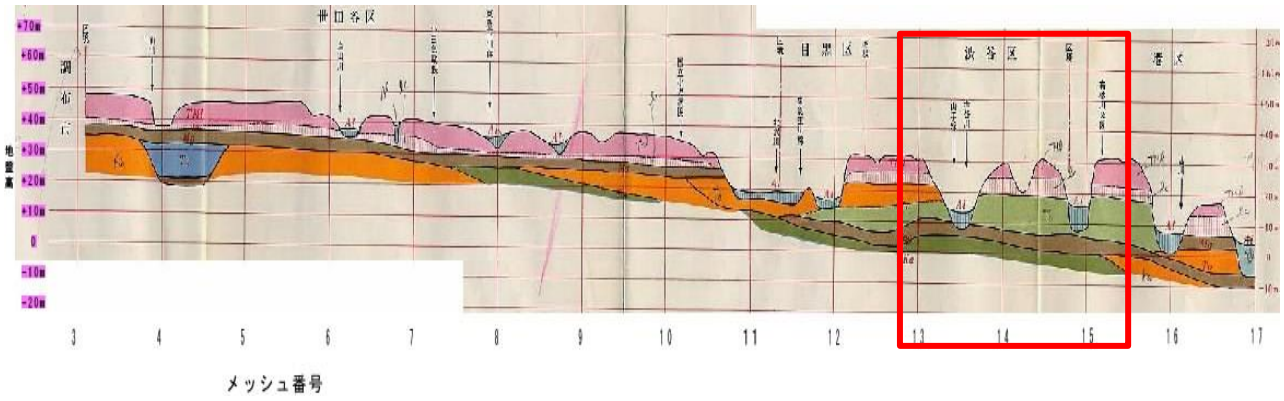


**Figure 4-14 Geologic cross section No. 17 (the left one in Figure 4-12, from website of the Bureau of Construction, Tokyo Metropolitan Government)[23]**

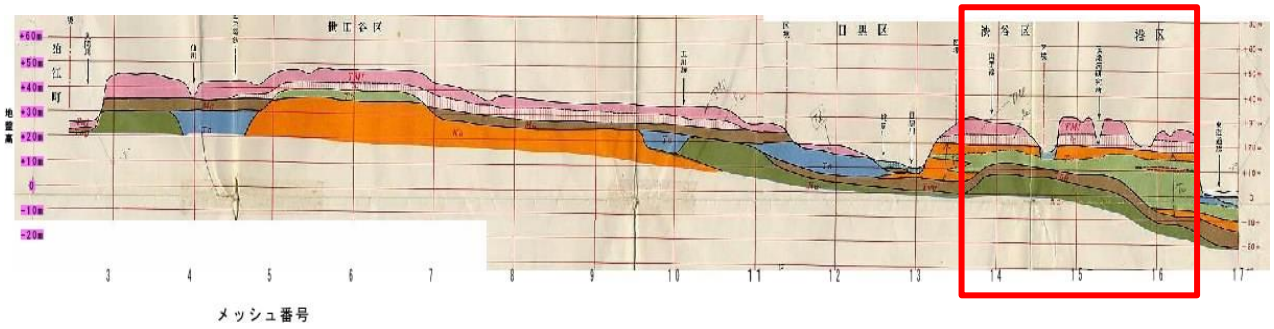


**Figure 4-15 Geologic cross section No. 18 (the left one in Figure 4-12, from website of the Bureau of Construction, Tokyo Metropolitan Government)[23]**

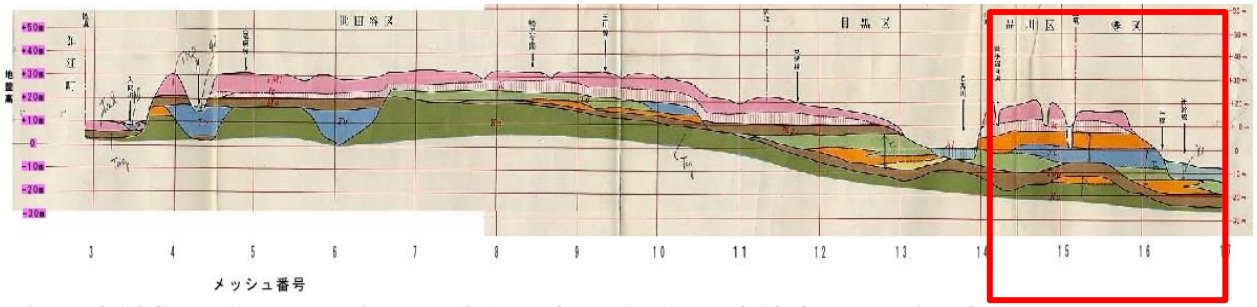


**Figure 4-16 Geologic cross section No. 19 (the left one in Figure 4-12, from website of the Bureau of Construction, Tokyo Metropolitan Government)[23]**


**Figure 4-17 A simplified geologic layering for the 3-D model**

The 3-D model was extruded from a plane polygon of the study area referring to the simplified local geologic layering initially, before elevation data for each geologic layer being given.

### 4.2.2 Elevation

Surface elevation data of each geologic layer was given to the model after the geologic layering setting being interpreted into FEFLOW model geometry.

The digital elevation model (10 m mesh, mesh No. 533934, No. 533935, No. 533944 and No. 533945) developed by the Geospatial Information Authority of Japan was interpolated into land surface, while for the surface of other geologic layers, elevation data were obtained from geologic cross sections and compiled into shape file maps via ArcGIS software (version 10.4, ESRI). The shape file maps loading elevation data were interpolated into the model layers.

### 4.2.3 Physical properties of strata and groundwater

In current 3-D model, since the study area locates in the same location with the 2-D cross section, both the model parameters and their values were set to be the same with the 2-D simulation. Hydraulic conductivities in Table 4-1 have been given for all the three directions in the

3-D model.

### 4.2.4 Temporal scenario

Current 3-D model was run following the time sequence as shown in Figure 4-18. The same with the 2-D cross section simulation, the "natural thermal state" of the stratum had been obtained before adding any boundary conditions for artificial constructions, and year 1945 has been set as the temporal zero point for the simulation. From this temporal zero point, the land surface temperature increase, namely subsurface UHI, was considered to begin.

Subsequently, inner heat sources corresponding to considered underground constructions were added to the model along the time line in which they have been opened. Conditions corresponding to subway line Tokyo Metro Hibiya Line was added to the model in 1964 (the 19$^{th}$ year in the simulation duration), following which the Tokyu Denentoshi Line, the Yamate Tunnel, and the Tokyu Toyoko Line were added in 1977, 2007, 2013, respectively (corresponding to the 25$^{th}$ year, the 32$^{th}$ year, the 62$^{th}$ year, and the 68$^{th}$ year in the simulation duration). Then the model was continuously run till year 2017 to predict current subsurface temperature distribution.

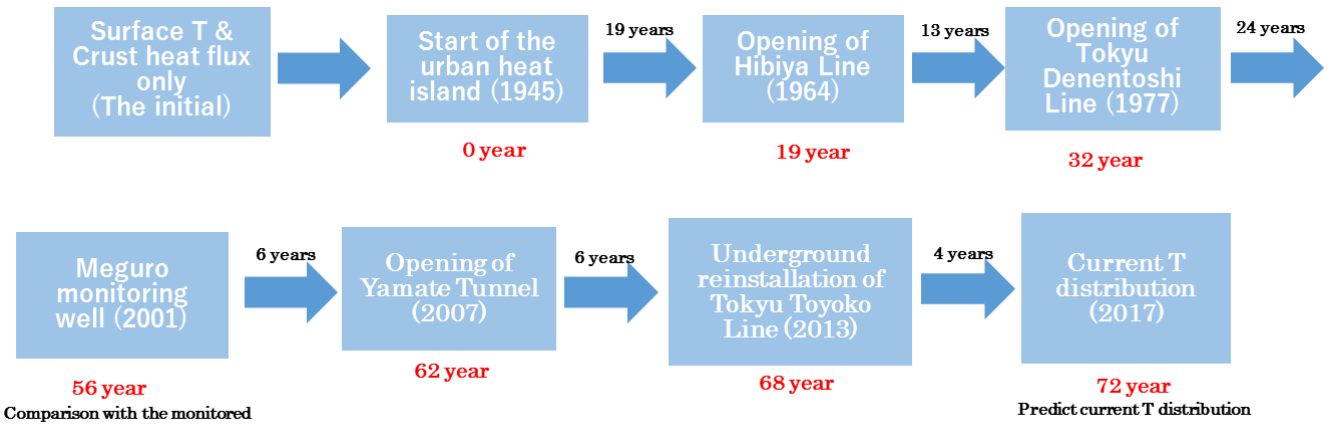


**Figure 4-18 Temporal scenario for the 3-D simulation**

To prevent the impact of unexpected flow to the subsurface temperature distribution, the hydraulic head was set as a same value for the whole model domain.

### 4.2.5 Boundary conditions for the urban heat island

In this part, UHI described as model conditions in the simulation are introduced. Generally, the subsurface UHI has been understood as the increase of land surface temperature and opening of artificial constructions in underground space (see Figure 3-9 and corresponding explanation). Hence underground construction boundary conditions and boundary condition for an increasing land surface temperature were designed for portraying the occurrence of subsurface UHI.

● The underground constructions

As introduced in 2.4, the subway line and the underground highway are considered in this study. They are given as inner heat sources to the simulation following the methods introduced below.

(1) The subway

Three underground railroads: Tokyo Metro Hibiya Line, Tokyu Denentoshi Line, and Tokyu Toyoko Line (the part from station Shibuya to station Daikanyama), locate in the study area.

Since the total amount of released heat and consequently a general subsurface temperature distribution instead of specific heat distribution near the constructions have been concentrated in this study, shape of the subway tunnels were omitted and the subway lines were simplified as line heat sources in current 3-D simulation for the convenience of model geometry building. Thermal influences of the subway lines to underground space have been captured the same way as that was in the 2-D cross section simulation introduced in 4.1.4, as temperature of the tunnel walls heating their surrounding strata. Monitor data of subway tunnel wall surface measured by Takeda [37] was used as an approximation for all the subway lines involved in this study, and was adapted to all the years of the simulation duration.

For the Hibiya Line, depths of all stations are available from literature (Figure 4-19)[40]. Average depth of the line, was calculated from averaging depth data of all the stations, and was given to the heat transport model to locate the line in strata. 12 m was used as an approximation of the calculated average depth, subjecting to the layer thickness of the model in its vertical direction.

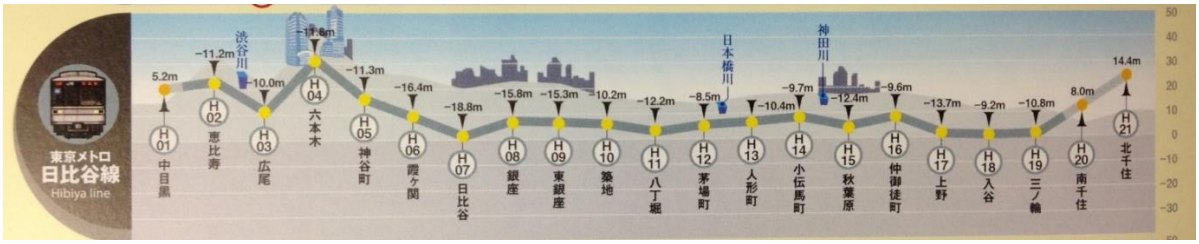


**Figure 4-19 Stations and their depths of Tokyo Metro Hibiya Line**[40]

In the case of Tokyu Denentoshi Line, average soil covering thickness of 6.93 m were figured out as the average depth of the line based on data in literature (Table 4-4)[41]. Practically, 8 m was given to the model subjecting to vertical layering of the model.

**Table 4-4 Soil covering thickness data of the tunnel of Tokyu Denentoshi Line**[41]

| No. | Thickness/m | No. | Thickness/m | No. | Thickness/m | No. | Thickness/m | No. | Thickness/m |
|---|---|---|---|---|---|---|---|---|---|
| 1 | 15.92 | 21 | 14.76 | 41 | 4.18 | 61 | 6.36 | 81 | 4.32 |
| 2 | 19.18 | 22 | 10.23 | 42 | 7.39 | 62 | 6.64 | 82 | 5.69 |
| 3 | 22.03 | 23 | 1.54 | 43 | 5.43 | 63 | 5.94 | 83 | 2.84 |
| 4 | 20.85 | 24 | 2.43 | 44 | 6.20 | 64 | 4.36 | 84 | 5.69 |
| 5 | 9.25 | 25 | 5.06 | 45 | 7.47 | 65 | 3.05 | 85 | 6.37 |
| 6 | 5.38 | 26 | 4.81 | 46 | 6.85 | 66 | 3.49 | 86 | 4.58 |
| 7 | 5.99 | 27 | 2.50 | 47 | 5.90 | 67 | 3.69 | 87 | 4.79 |
| 8 | 5.09 | 28 | 4.06 | 48 | 5.37 | 68 | 4.35 | 88 | 3.19 |
| 9 | 2.58 | 29 | 3.36 | 49 | 6.90 | 69 | 6.74 | 89 | 4.57 |
| 10 | 3.71 | 30 | 2.68 | 50 | 9.22 | 70 | 3.26 | 90 | 7.35 |
| 11 | 13.65 | 31 | 2.71 | 51 | 10.09 | 71 | 3.16 | 91 | 6.76 |
| 12 | 15.64 | 32 | 1.95 | 52 | 10.59 | 72 | 3.20 | 92 | 4.51 |
| 13 | 17.68 | 33 | 2.82 | 53 | 9.11 | 73 | 3.16 | 93 | 3.32 |
| 14 | 19.71 | 34 | 2.08 | 54 | 7.14 | 74 | 6.08 | 94 | 0.85 |
| 15 | 19.20 | 35 | 1.37 | 55 | 3.27 | 75 | 4.46 | | |
| 16 | 18.53 | 36 | 2.75 | 56 | 6.67 | 76 | 3.16 | | |
| 17 | 17.63 | 37 | 1.41 | 57 | 6.83 | 77 | 3.30 | | |
| 18 | 16.05 | 38 | 3.23 | 58 | 6.94 | 78 | 3.35 | | |
| 19 | 17.08 | 39 | 4.70 | 59 | 6.94 | 79 | 4.82 | | |
| 20 | 17.12 | 40 | 3.09 | 60 | 6.47 | 80 | 5.02 | | |

For the Tokyu Toyoko Line, the section from station Shibuya to station Daikanyama has been reinstalled underground, with maximum soil covering thickness of 15.7 m and minimum soil covering thickness of 4.7 m (Figure 4-20)[29]. The maximum and minimum values of soil covering thickness were averaged to obtain the average depth of the tunnel. Such approximation of tunnel depth was considered reasonable here because that even in current stage the model is not yet reliable, but finally, the purpose of the model is to discuss geothermal potential and utilization of the heat released by underground constructions, and obviously, geothermal utilizing facilities cannot be installed impaling a railway tunnel. Average depth of tunnel calculated by the aforementioned approach is 10.2 m, and 10 m was given to the model based on the vertical

layering of the model.

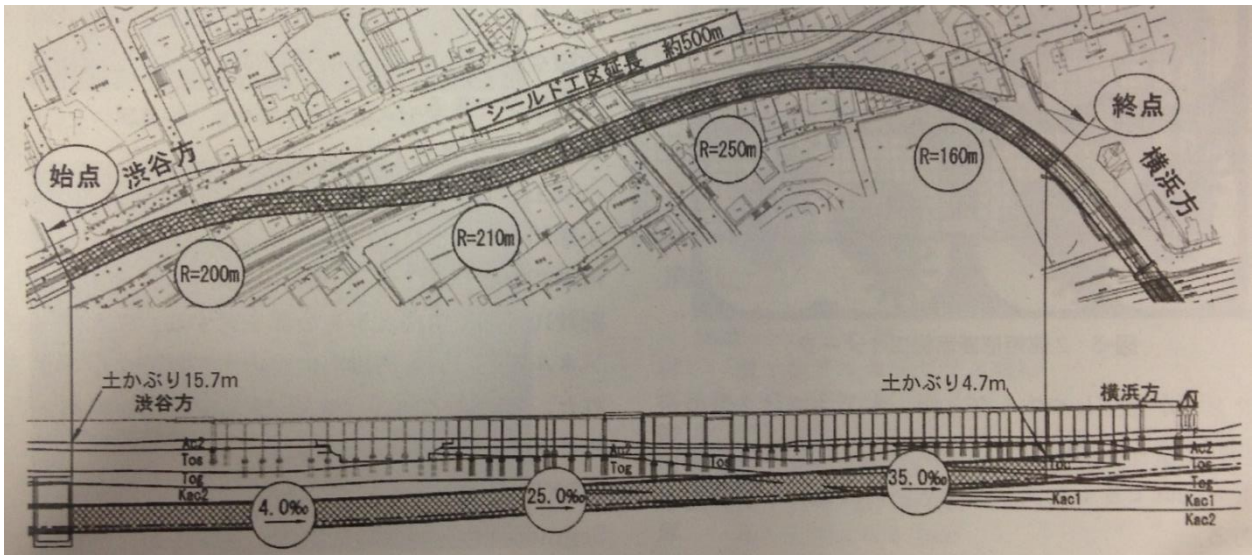


**Figure 4-20 Ichnography and profile of shield construction along Shibuya to Daikanyama section, Tokyu Toyoko Line**[29]

(2) The Yamate Tunnel

Yamate Tunnel is an underground highway tunnel crossing the study area. The same with the subway case, the tunnel was simplified as a line heat source, representing the tunnel wall. Surrounding space was considered to be heated by the tunnel wall temperature.

Temperature of the tunnel wall was measured by Yazaki (Figure 4-21)[31]. However, time scale of the measurement has not been given in the report. Hence to infer the time scale of the aforementioned measurement, a comparison between air temperature inside and outside of the tunnel from the same report has been referred to (Figure 4-22)[31]. Air temperature out of the tunnel fluctuates at a period of 1 day, and air temperature inside the tunnel oscillates almost the same period, as shown by Figure 4-22. Furthermore, in Figure 4-21, it has been observed that temperature of the tunnel wall changes right after air temperature inside the tunnel. Thus, it can be concluded that Yazaki's measurement had lasted for around 18 days, which means daily change of the tunnel wall temperature was captured. Heat transport model in this study has been designed to compare the change in temperature distributions at different scenarios, which aims at generalized temperature distribution results instead of a series of precise results at certain time steps of a single simulation. So as a very initial stage, the average tunnel wall temperature (around 36.3 ℃) was

taken as the model input.

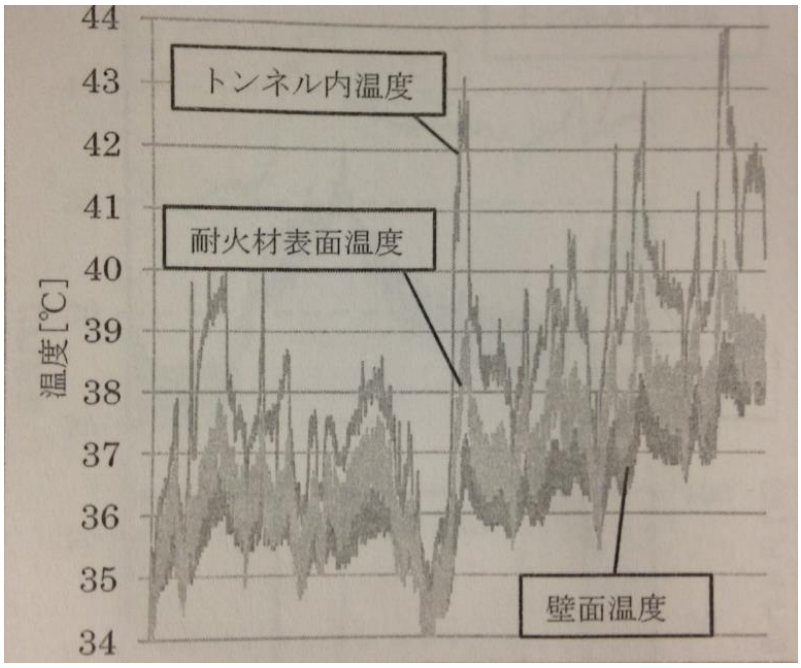


**Figure 4-21 Measured temperature fluctuation of the tunnel wall, the fire resistant material, and the air inside the tunnel**[31]

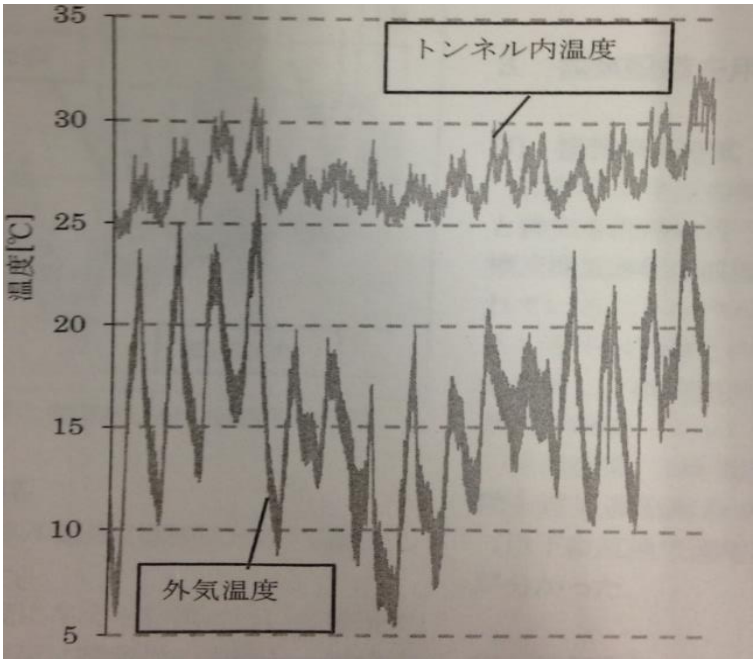


**Figure 4-22 Measured air temperature fluctuation inside and outside the tunnel**[31]

Average depth of the tunnel was calculated by taking an average of the maximum soil covering thickness and the minimum soil covering thickness (Figure 4-23)[42]. Depth of the tunnel was given as 30 m in the model.

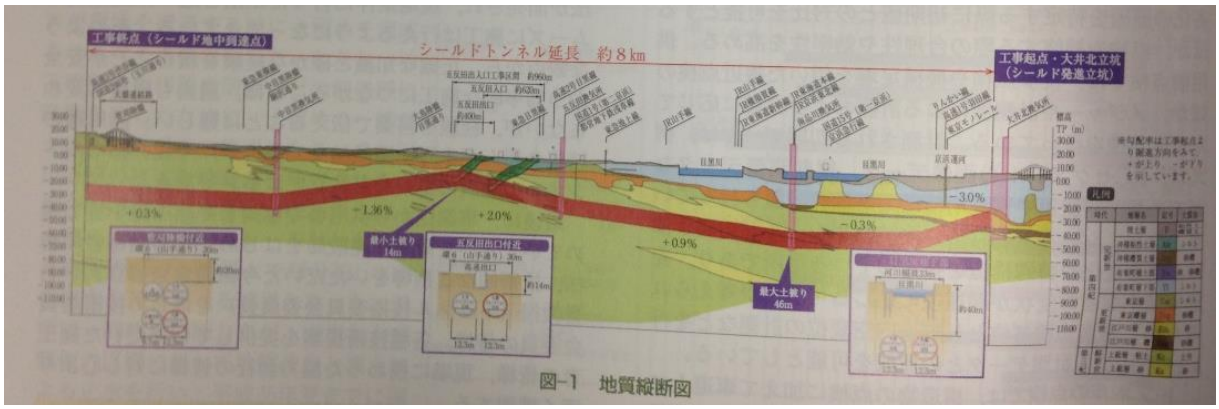


**Figure 4-23 Profile of the Yamate Tunnel, the maximum and minimum soil covering thickness are marked by purple bubble in the graph**[42]

●The land surface temperature and its increase

In the land surface temperature section, UHI means an increase of the surface temperature.

Since several land use type exists in the study area and changes along time as introduced in 2.3, here the land surface temperature expression for each type of land use is obtained firstly, before any increase is considered. Using the same approach adopted for the land surface temperature of the 2-D cross section, Formula 4-1 has been referred to as a paradigm, to which an increasing rate of land surface temperature was added.

Measured daily temperature changes of different land surface textures have been reported by literature (Figure 4-24)[43]. Amplitude for each type of land surface temperature has been decided from the graph (Figure 4-24), and period of 1 day, the same period with the monitored data, has been set to plot the surface temperature functions written initially (Formulas 3-10~ 3-12). By comparing the relative locations of the plotted graphs and corresponding literature graphs in the time axis (the horizontal axis), the phase constant has been calibrated. Finally, land surface temperature without considering temperature increase for asphalt surface, concrete surface, bare-land surface and grass-land surface were written as Formula 4-3~ 4-5, respectively.

$$T_{concrete}(0,t)=16+22\sin\left(\frac{2\pi t}{\tau}-\frac{\pi}{2}\right) \quad (4\text{-}3)$$

$T_{bare\ land}(0,t)=14+21\sin\left(\frac{2\pi t}{\tau}-\frac{\pi}{2}\right)$ (4-4)

$T_{grass\ land}(0,t)=14+18\sin\left(\frac{2\pi t}{\tau}-\frac{\pi}{2}\right)$ (4-5)

$T_0$: *Average land surface temperature, ℃;*

$A_0$: *The amplitude of land surface temperature, ℃;*

$\tau$: *The period of land surface temperature, day;*

$\varnothing$: *Phase constant, day*

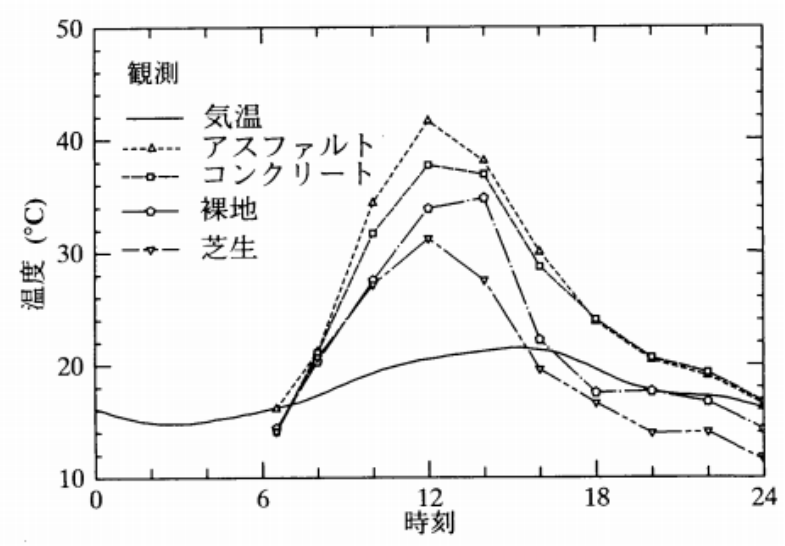


**Figure 4-24 Measured daily temperature change of air, asphalt surface, concrete surface, bare land and grass land** [43]

Similar to the 2-D case, a land surface temperature increase rate of 2/52 ℃/year (see "the boundary condition" in 1.4.1 for derivation) was added to the temperature functions. However in the current 3-D case, the unit of the increase rate has been converted to ℃/day. This is because that 1 day has been set as the period for temperature change here in the 3-D case ($\tau$= 1 day). Hence, the land surface temperature with UHI considered were written as Formulas 4-6~ 4-8, for each type of land use respectively.

$T_{concrete}(0,t)=16+22\sin\left(\frac{2\pi t}{\tau}-\frac{\pi}{2}\right)+\frac{1}{1825}t$ (4-6)

$T_{bare\ land}(0,t)=14+21\sin\left(\frac{2\pi t}{\tau}-\frac{\pi}{2}\right)+\frac{1}{1825}t$ (4-7)

$T_{grass\ land}(0,t)=14+18\sin\left(\frac{2\pi t}{\tau}-\frac{\pi}{2}\right)+\frac{1}{1825}t$ (4-8)

As showed in Figure 4-18, the simulation time started from year 1945 and ended in year 2017. Referring the time period to the timeline of land use change in the study area, it can be described that the timely change of land use in the simulation duration is as follows: from the beginning time of the simulation, the study area was almost used as a farm land, with only area near the railway urbanized. The urbanized area was found to be extended in the 1st year of the simulation. When the 30th year of the simulation time came, farm land has disappeared in the study area and its vicinity, while urbanized area was extending from the central zone of Tokyo Metropolitan to suburban villages.

Here in this study, villages as bare land surfaces, farm land as grass land surface and urbanized area as concrete surface have been roughly assumed, respectively. As a model boundary condition, land surface temperature change during year 1945~ 2017 corresponding to land use change was given.

●The crustal heat flux

Crustal heat flux was thought to be relatively stable, thus 0.03 W/m$^2$ (0.76 HFU, see Figure 4-10 and its corresponding explanation) was given to all of the scenarios.

### 4.2.6 Groundwater flow

Groundwater flow is the main control factor in this study. Subsurface temperature distributions with and without the influence of groundwater flow were compared to inspect the influence of groundwater flow to subsurface temperature distribution. In this section, groundwater flow described as model conditions in the simulation are introduced first, and then follows introduction on how the condition will change when the groundwater flow factor being turned off.

As introduced in 3.2.1, groundwater flow in the study area has been simulated at steady-state to obtain a generalized hydraulic head distribution of the study area along years. To reproduce the local hydraulic head distribution, infiltration boundary condition (flux entering into the model domain), river boundary condition (fixed head, a 1st kind boundary condition. Cooperating with

the flux/2nd kind boundary condition, the model will be more stable), and discharge boundary condition (flux draining out from the model domain) have been defined respectively.

Average rate of precipitation infiltrating into underground in Japan was reported as 1 mm/day[20]. This value was given as the infiltration boundary condition to current groundwater flow simulation. Water depth in the Meguro River (< 0.5 m)[21] is not so significant compared with local groundwater level data in literature (around 14 m)[26], hence here in this study, river bed elevation has been used as an approximation of the river water level (also, the local groundwater level), and was given as the fixed head boundary condition. Since tributaries of the Meguro River were reinstalled underground as sewage culverts before 1962[44], which means that digital elevation model reflects the elevation of the culvert cover instead of the river water level (see Figure 4-25 for image). Thus, an old map (1896~1909)[45] has been read to track the river bed elevation for the river fixed head boundary. As mentioned earlier, flow in the Meguro River is very small (see 2.2). So for convenience of model calculation, here it has been assumed that the river receives water mainly from precipitation instead of their upstream, and in this way, side boundary of the model has been set as no groundwater flow. As an exception, there is water draining out of the model domain from the rivers. Assume water mainly drains from Meguro River, which is the main river in the study area. Then Darcy flow of the Meguro River and the Shibuya River were added together to form a total draining flow of the study area. The flow draining out from the model domain was specified as 0.03 m/day by applying Darcy's Law to hydraulic conductivity of the aquifer and an average head gradient of the river.

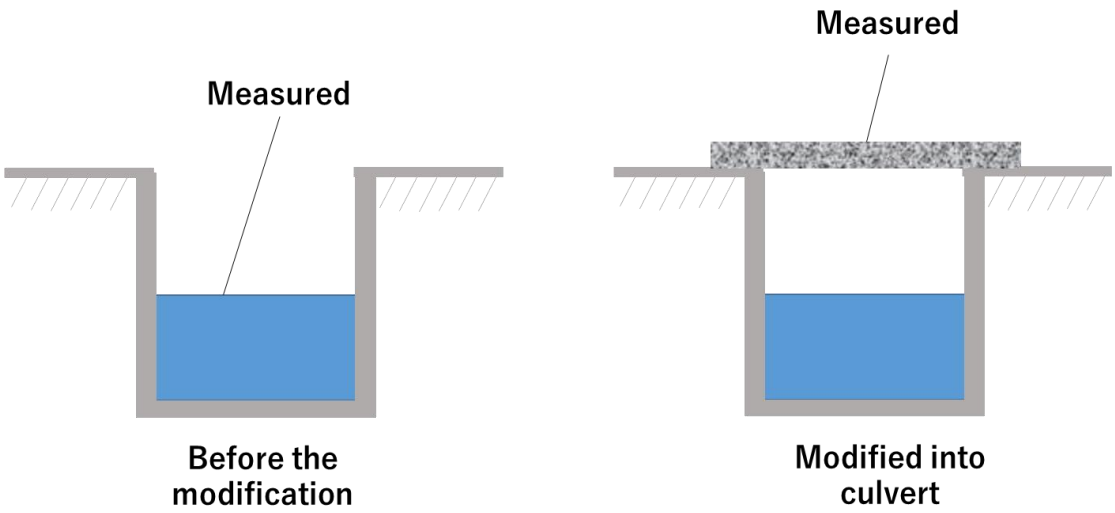


**Figure 4-25 A schematic figure for the measured data of the digital elevation model before and after the river being modified into a culvert**

For designed scenarios considering the factor of groundwater flow, contour result calculated form the aforementioned settings were fixed as a head distribution to the corresponding simulation; while for those scenarios without consideration of groundwater flow, the hydraulic head was set as a same value for the whole domain to prevent the occurrence of groundwater flow.

# 5 Results and discussions

In this chapter, simulation results of current study are compared with monitored data to discuss the quality of simulations. Firstly the 2-D result is compared with a monitored subsurface temperature profile to check the modeling approach. For the 3-D model, the calculated groundwater contour is compared with a measured one to inspect the flow simulation, while the calculated subsurface temperature is estimated by comparing with a measured profile. Finally, temperature distributions under UHI considering and excluding groundwater flow factor are compared with each other to discuss the influence of groundwater flow to subsurface temperature distribution.

## 5.1 Comparison of the calculated results with monitored data

### 5.1.1 2-D model

Subsurface temperature distribution in a 2-D cross section heated by a subway tunnel was simulated under the assumption of UHI (thus, an increasing land surface temperature) to obtain a modeling approach, which is expected to be able to abstract subsurface temperature distribution influenced by groundwater flow in the real into 2-D rectangle models and further 3-D box models. The calculated subsurface temperature profile was compared to a monitored one measured at the Meguro Monitoring Well (see Figure 5-1 for location in map, and Figure 5-2 for location in the cross section) on 6$^{th}$, Nov., 2001 to estimate the model quality (Figure 5-3). Direction of local groundwater flow is marked in Figure 5-1.

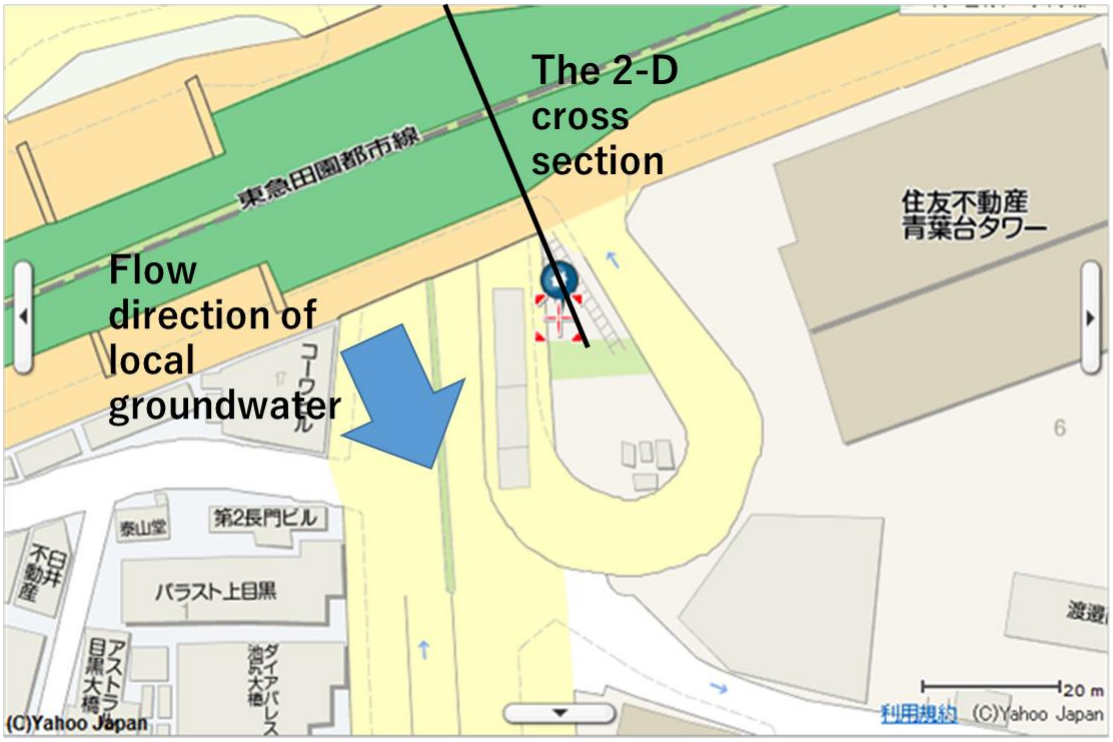


**Figure 5-1 Location of the Meguro Monitoring Well in map (Adapted from Fujii, 2010)**[7]

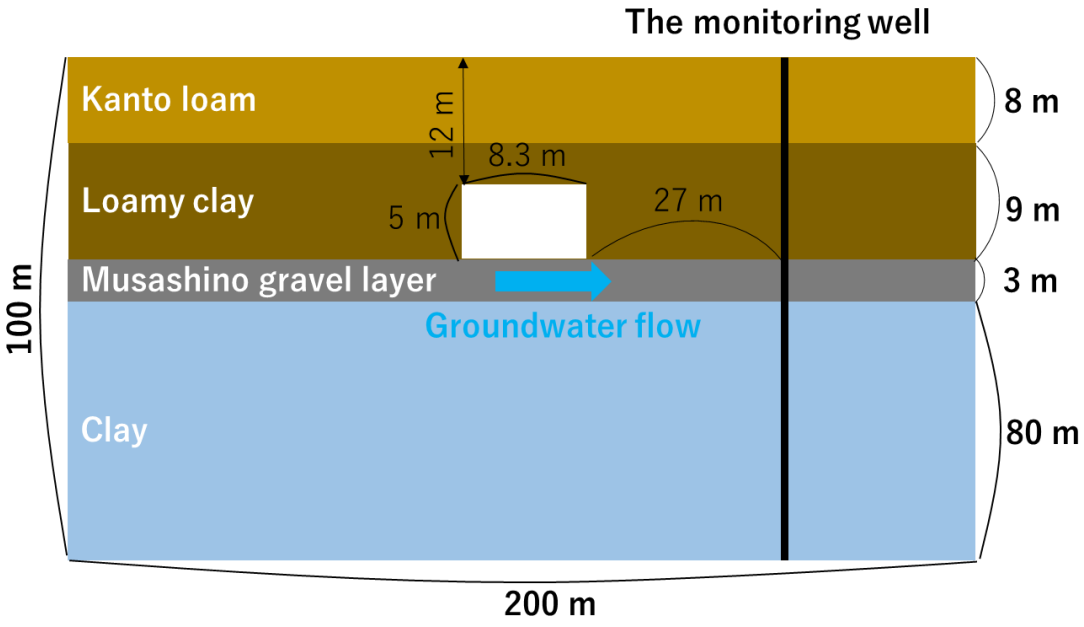


**Figure 5-2 Location of the Meguro Monitoring Well in the cross section (Adapted from Fujii, 2010)**[7]

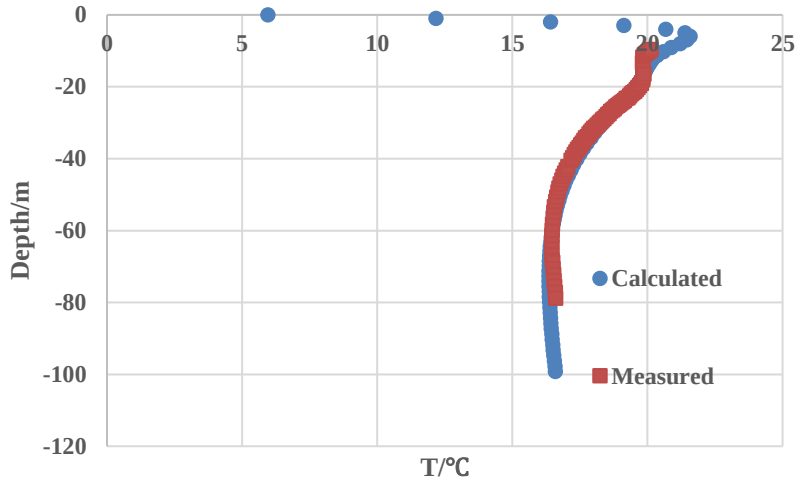


**Figure 5-3 A comparison between the 2-D simulation result and the measured data (source of the measured profile: Fujii, 2010[7])**

Observing the calculated temperature profile, it can be observed that the subsurface temperature near land surface is low for both the with-flow result and the no-flow result. This is because that current result represents winter time, during which temperature near land surface is low itself. The subsurface temperature increases significantly at the depth of around -5 m, then decreases gradually until reaching a similar level with the measured temperature profile, to around 16.5 ℃.

In current discussion on the 2-D cross section, temperature near land surface, temperature near the underground construction, and temperature at the deepest place of the profiles are inspected respectively to prove the reliability of the modeling approach.

From a calculation on seasonal change of subsurface temperature profiles without human disturbance (Figure 5-4[7]), it can be known that the influence of land surface temperature can reach 10 m downward into underground space, and peaks of subsurface temperature profiles appear at the depth less than 5 m from the surface. Thus the significant temperature increases of the calculated results at -5 m very possibly reflect the influence of land surface temperature. Compare the temperature values at the peak of the calculated results and the literature profile, it can be found that peak of the calculation is approximately 5 ℃ higher than the peak of literature profile, which is right the temperature increase given to the land surface boundary condition to portray the influence of UHI phenomenon to land surface temperature. In this way, it can be concluded that current modeling approach can well reflect the land surface temperature increase caused by UHI.

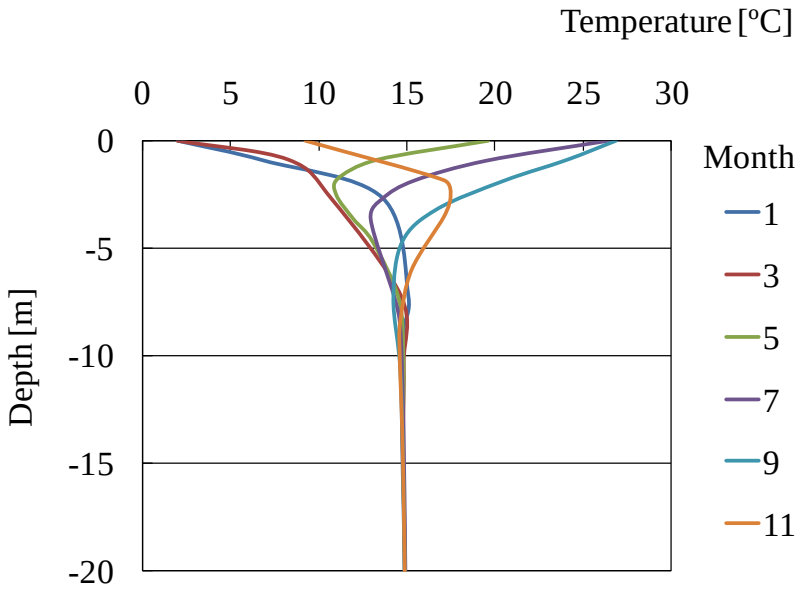


**Figure 5-4 Seasonal change of subsurface temperature profiles without urban heat island**[7]

Then for temperature near the underground construction (around – 20 m), a temperature increase has been seen in the measured temperature profile. This is considered to be caused by the heating of the subway tunnel[7]. At the same depth, the calculated profile matched well with the measurement, proving that current modelling approach can catch the influence of underground constructions to subsurface temperature.

Furthermore, observing shape of the profiles at their deepest place, it can be observed that subsurface temperature gradient of the measured profile was well reproduced by the calculation, even the absolute value of calculated temperatures still have a little offset (around 0.3 ℃) with the measured data yet (Figure 5-5). Hence the modeling approach reproduced the subsurface temperature profile quite well.

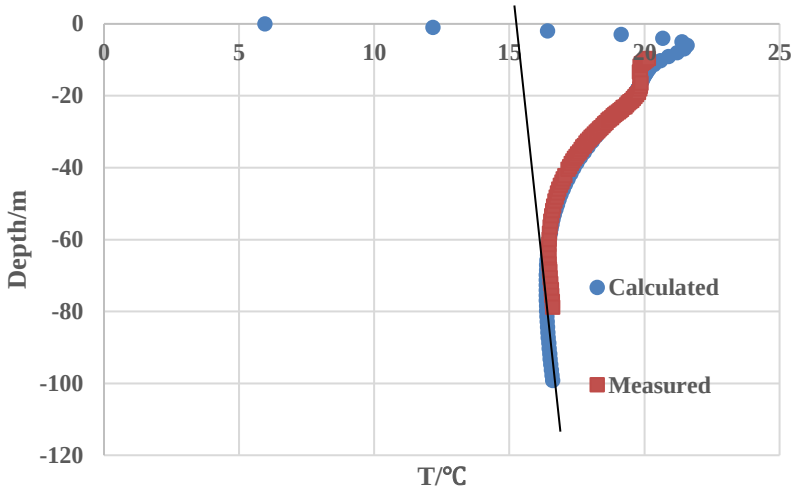


**Figure 5-5 A comparison between the calculated subsurface temperature gradient and the measured one (source of the measured profile: Fujii, 2010[7])**

In short, the 2-D cross section model can successfully reflect the land surface temperature increase caused by UHI, catch the temperature change caused by underground constructions, and reproduce the measured subsurface temperature gradient.

### 5.1.2 3-D groundwater flow

Using the built 3-D model, steady-state groundwater flow simulation was conducted to obtain a generalized groundwater contour in the study area, as an initial hydraulic head input for further simulating the groundwater-flow-influenced subsurface temperature distribution under UHI. In this section, the calculated groundwater contour map (Figure 5-6) is compared with a measured one (Figure 5-7) to estimate the flow simulation.

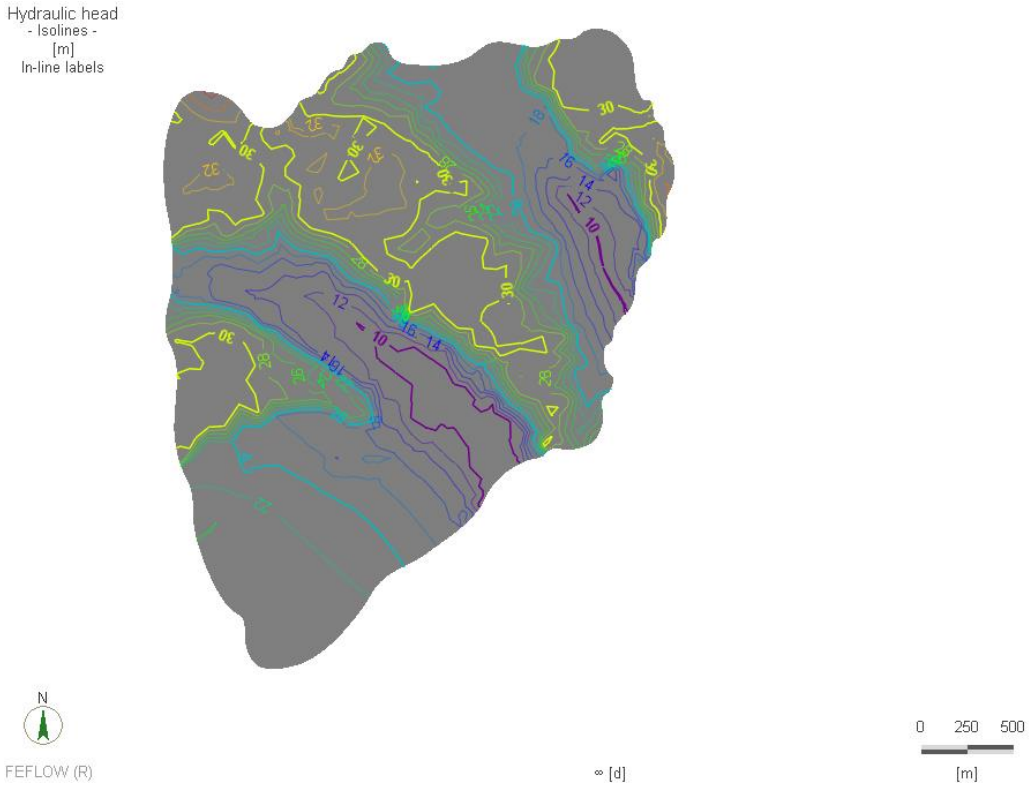


**Figure 5-6 The calculated groundwater contour map**

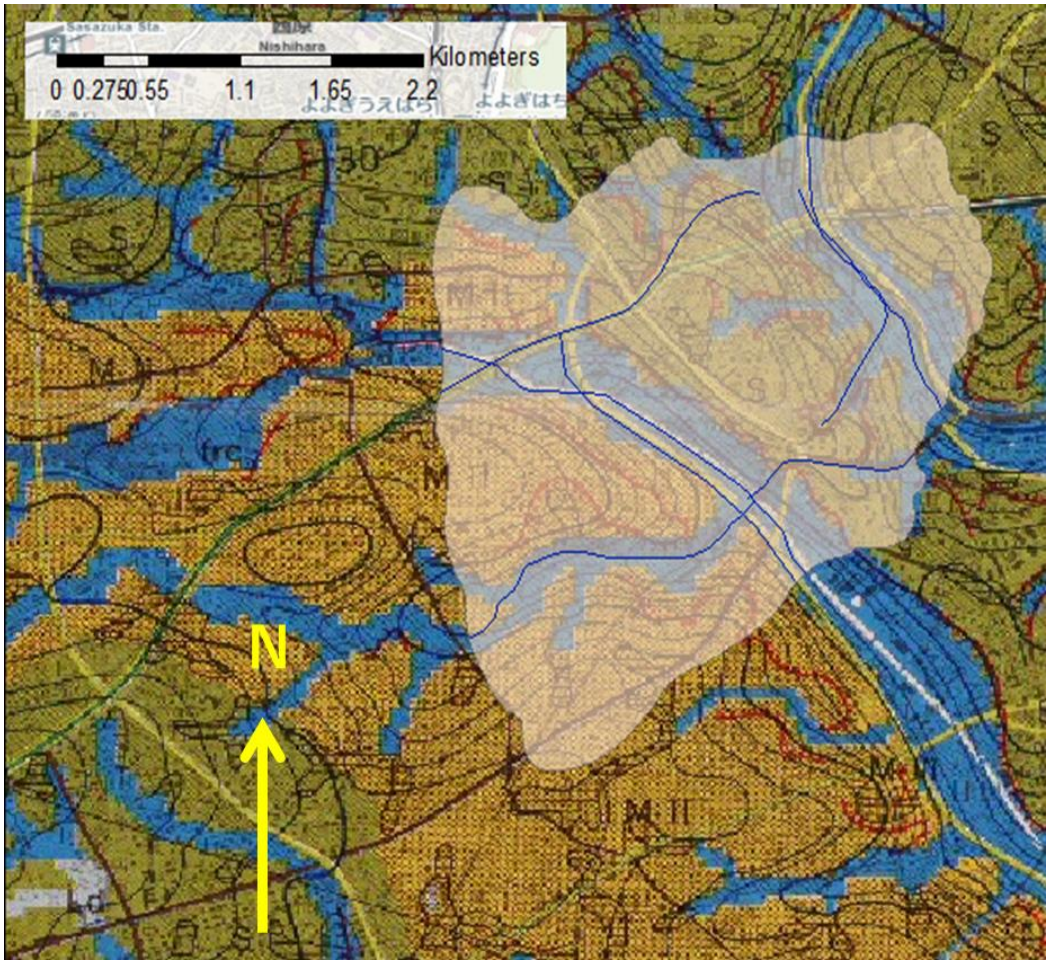


**Figure 5-7 The measured groundwater contour (adapted from the landform classification map, Ministry of Land, Infrastructure, Transport and Tourism)**[16]

As it can be observed from the calculated contour (Figure 5-6), the highest hydraulic head appeared in the hills locate in the northeast, southwest and center of the study area as 30 m, sandwiching river beds where the lowest hydraulic head of 10 m appeared. The shape of the calculated contour resembles the measured one very much in shape, indicating that the steady-state flow simulation can preferably reproduce the hydraulic head distribution of the local groundwater. Besides, a measured datum of groundwater level was compared with the calculated one to further inspect the calculated groundwater level. The groundwater level datum was measured at the location showed in Figure 5-8, and the value is around 13.5 m[26]. Calculated groundwater level at that point is 14 m (Figure 5-6), indicating a well reproduction of the groundwater level by the steady-state groundwater flow simulation.

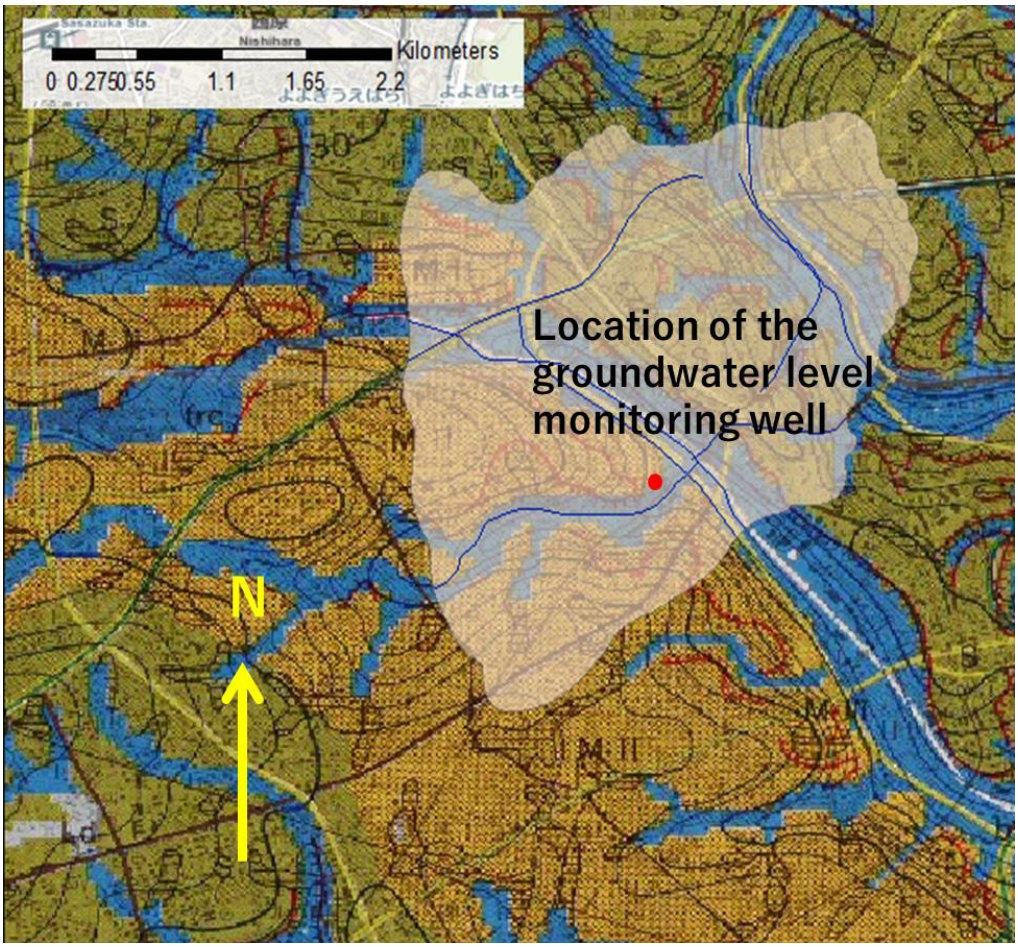


**Figure 5-8 Location of the groundwater level monitoring well in the study area (adapted from the landform classification map, Ministry of Land, Infrastructure, Transport and Tourism)**[16]

### 5.1.3 3-D subsurface temperature

Subsurface temperature was simulated in the built 3-D model. Temperature profile at the location of Meguro Monitoring Well has been extracted at the time step corresponding to the measurement (6th, Nov., 2001) to estimate the simulation quality (Figure 5-9).

Generally, the fitting of the calculated profile to the measured one needs further improvement. However, the influence of underground construction to subsurface temperature and the subsurface temperature gradient were somehow reproduced. In this way, here it is considered that result of the 3-D subsurface temperature simulation is acceptable.

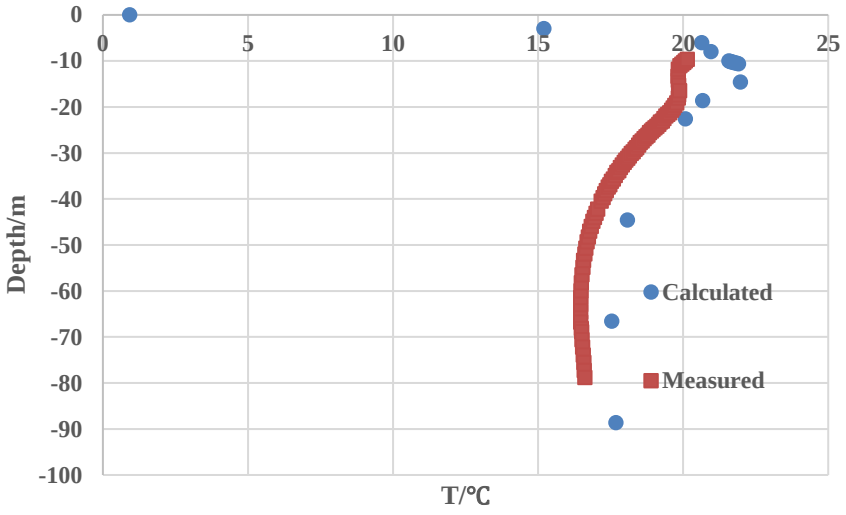


**Figure 5-9A comparison between the 3-D simulation result and the measured data (source of the measured profile: Fujii, 2010[7])**

## 5.2 Influence of groundwater flow

To inspect influence of groundwater flow to subsurface temperature, the temperature profile calculated with groundwater flow was compared with the result calculated without groundwater flow for both the 2-D model (Figure 5-10) and the 3-D model (Figure 5-11) firstly.

At depth of -20 m, which is right beneath the subway tunnel, and is the depth of aquifer where groundwater flows, for the profiles including influence of groundwater flow, the temperatures is equivalent to the measurement in the 2-D case, and is higher than the measurement in the 3-D case; while for the profiles excluding the influence of groundwater flow, the temperatures are lower than the measurement. Since the monitoring well locates downstream of the subway tunnel, it is considered that groundwater flow carries heat released by the subway tunnel to the monitor well, making the temperature there become higher. Thus it is considered that the temperature difference caused by groundwater flow can be well caught both by the 2-D model and the 3-D model, even the general fitting of the 3-D result is not perfect yet.

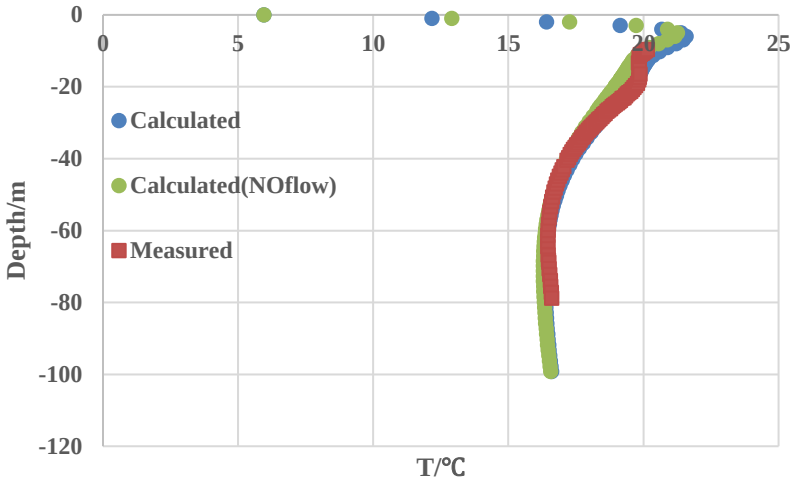


**Figure 5-10 A comparison of subsurface temperatures calculated by the 2-D cross section model (source of the measured profile: Fujii, 2010[7])**

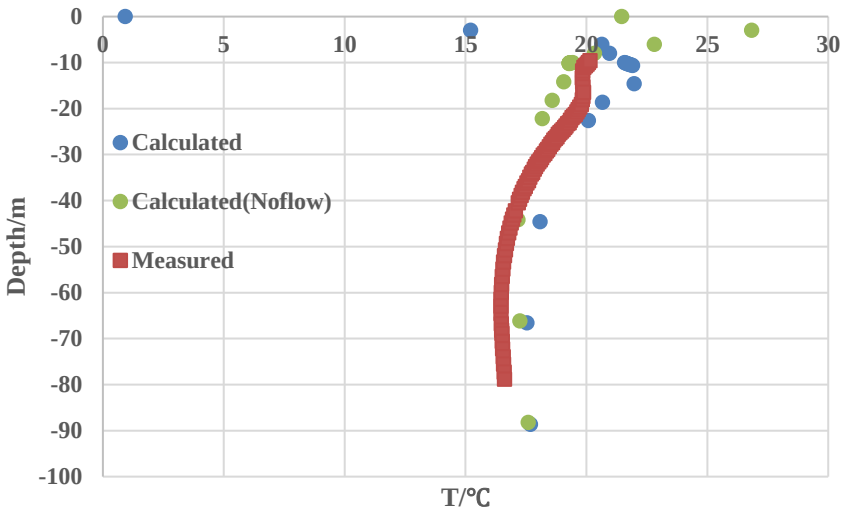


**Figure 5-11 A comparison of subsurface temperatures calculated by the 3-D cross section model (source of the measured profile: Fujii, 2010[7])**

Since current model can provide effective information on the influence of groundwater flow to subsurface temperature, a comparison between the temperature distribution calculated from the with-flow case and the result from no-flow case were conducted to discuss the influence of groundwater flow to subsurface temperature distribution (Figure 5-12). For the temperature distribution result, data at the average depth of Musashino Gravel Layer (–16 m), which is the main aquifer in the study area, have been taken for the comparison.

Generally, subsurface temperature is approximately 17.3 ℃ in most part of the study area

when groundwater flows, while for the case without groundwater flow, subsurface temperature in most part of the study area is around 19.8 ℃.

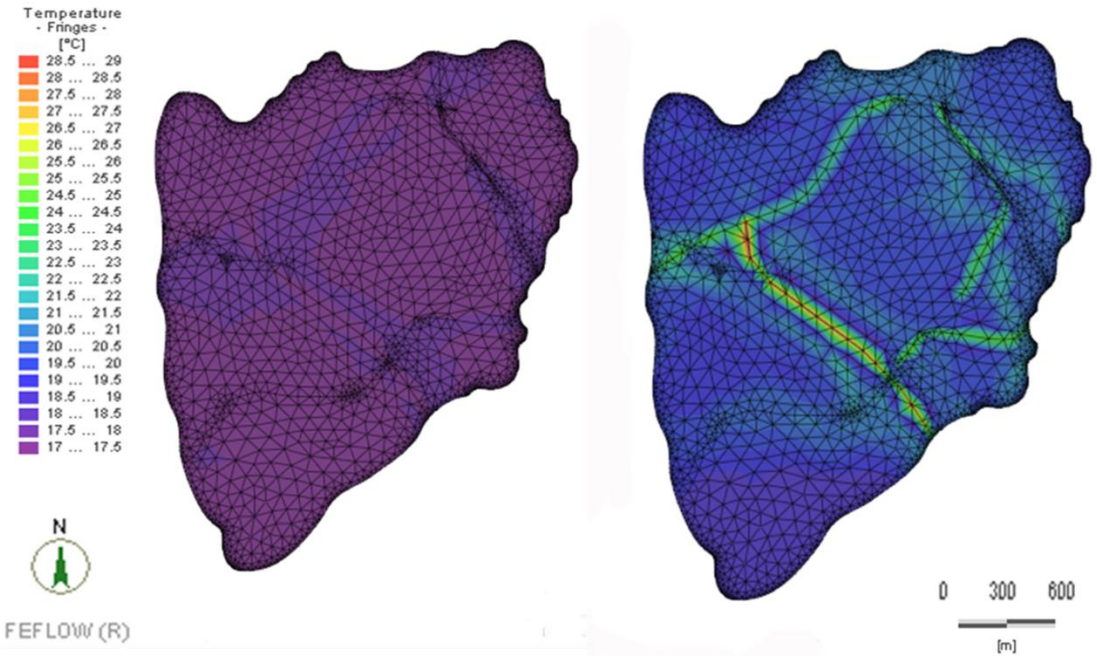


**Figure 5-12 Calculated result of UHI-influenced subsurface temperature distribution (Left) with the influence of groundwater flow and (Right) without the influence of groundwater flow**

Comparing the left and the right in Figure 5-12, it can be observed that in the case with groundwater flow, high temperature area extended from the location of inner heat sources (see Figure 2-9 for locations of the heat sources, and Figure 5-13 for groundwater flow direction in the study area) to larger area along the direction of groundwater flow, while in the case without groundwater flow, high temperature area is fixed near the heat sources. Besides, a temperature decrease of near 3 ℃ in most part of the study area has been observed when groundwater flow appears in the study area. Hence groundwater flow do influence the distribution of subsurface temperature, not only lowering general level of temperature, but will carry heat downstream, enlarging influence range of the heat sources as well.

Shortly, current 3-D flow-UHI joint model can well catch the influence of groundwater flow to subsurface temperature. Groundwater flow lowers general level of temperature, but will carry heat downstream, enlarging influence range of the heat sources.

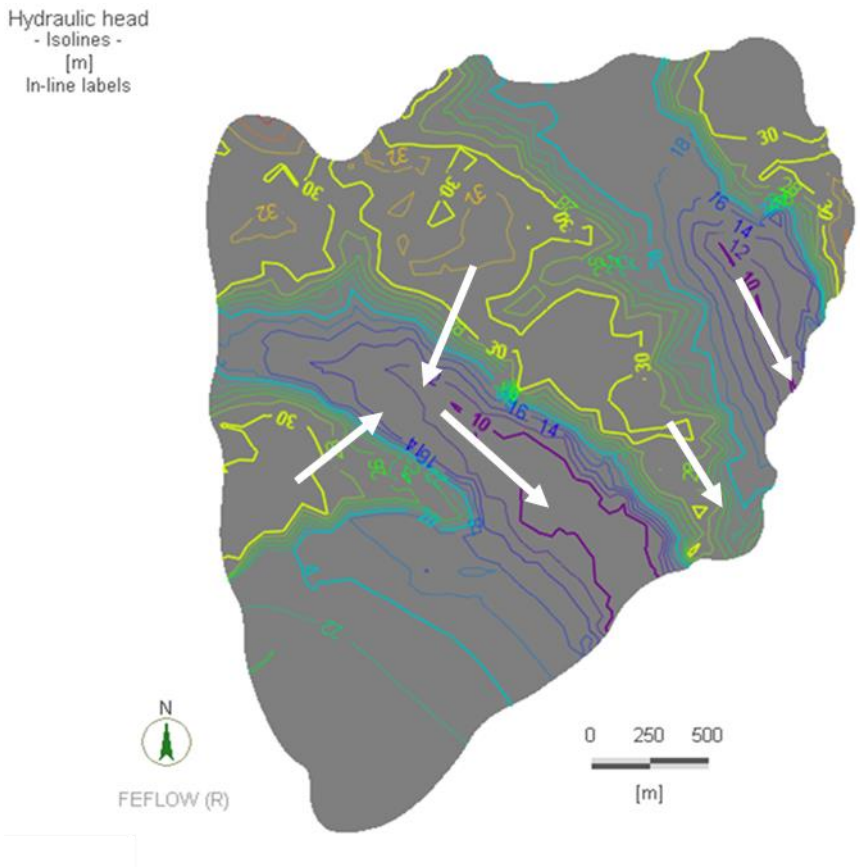


**Figure 5-13 Calculated flow direction of groundwater in the study area (white arrows represent the direction)**

# 6 Conclusions and outlook

To improve the accuracy of anthropogenic heat simulation, a trial on building a 3-D flow-UHI joint model has been made. A 2-D cross section model was built initially for obtaining the modeling approach, after which model dimension was extended into 3-D. Then local groundwater contour was obtained via a steady-state flow simulation, and the result was fixed into the UHI-considered simulation for subsurface temperature to simulate the flow-influenced temperature distribution. For inspection of the influence of groundwater flow, temperature distribution was also obtained under the condition in which a fixed head had been given to the whole model domain to prevent groundwater from flowing. Reliability of current modeling approach, quality of the 3-D flow simulation and the 3-D flow-UHI joint simulation were estimated respectively. Finally temperature distribution with and without the influence of groundwater flow were compared to each other.

It has been concluded that (i) current modeling approach used to catch subsurface temperature distribution influenced by groundwater flow is reliable, that the 3-D model can well reproduce groundwater flow in the study area and can reflect influence of groundwater flow to subsurface temperature; (ii) groundwater flow do influence subsurface temperature distribution, one way by lowering general level of temperature, the other way by carrying heat downstream, enlarging influence range of the heat sources. Hence the approach here in this study is considered helpful to improve the accuracy of mapping the heat stock of subsurface UHI.

For further improvement of the model, sewage system is better added as artificial heat source for a more realistic approximation of the underground thermal environment (a possible method dealing the sewage heat source was discussed, and was attached to the thesis as an appendix).

**Acknowledgement**

At the time point when the thesis is to be finished, the author would like to first appreciate sincerely to her supervisor, Professor TOKUNAGA Tomochika, for all his patient instructions and always being inspiring and supportive not only for the research, but also for life. Also, the author is grateful to her co-advisor, Assistant professor AICHI Masaatsu, who has lent computer in his lab generously for the research and provided very helpful advises on current study.

Besides, the author wants to thank to Dr. ITO Yuka for her kind advices on the thesis and ArcGIS problems; Mr. LIU Jiaqi for always kindly providing discussions on the FEFLOW software; Mr. MOGI Katsuro for his supporting on computer resources; Mr. URAKOSHI Takuya for kindly providing railway-tunnel-related material; Associate professor SATO Hiroyasu from the Department of Socio-Cultural Environmental Studies for warmly providing advices and materials on sewage-system-related assumptions; Mr. HADA Makoto at DHI, Japan for patiently instructing the author on FEFLOW software through mail.

Finally, last but not least, the author wants to say thank you to all the lab members, for their comments on the research during the lab seminar and all their support in daily life; also, to families and friends for their warm encouragement and always being by my side.

## Appendix

A-1 Definitions of physical properties of the strata

*Porosity:* The percentage of the rock or soil that is void of material

*Saturation:* The volume of the contained water divided by the total volume of the soil

*Hydraulic conductivity:* The ability of a material to conduct flow

*Thermal conductivity:* The ability of a material to conduct heat

*Heat capacity:* The ability of a material to storage heat

*Bulk density:* The soil density counted by both the liquid and solid material

*Solid density:* The density of solid body of the soil

A-2 Abbreviations

UHI: urban heat island

REA: representative elementary area

REV: representative elementary volume

A-3 A discussion on sewage system heat source

The density of sewage system in the study area, which locates in the special wards of Tokyo, is quite high as shown by Figure A-1. Thus considering convenience of building the model geometry, the local sewage system have been treated as a plane heat source in the model, and a spatial average heat flux released by the plane heat source was derived following the procedure below.


**Figure A-1 Covering condition of sewage system (trunk lines) of Meguro Ward, crossing which the study area locates**[46]

To figure out the spatial average heat flux, first consider the heat flow released by the sewage pipes per meter entering into underground space in a REV (Figure 3-3 (B)). The process that heat transports from the sewage system into strata can be explained by the heat transfer between the sewage water and the pipe wall. Since temperature distribution in the strata but not the sewage pipe is the core of interest in this study, heat flowing from the sewage system into the strata has been set as the positive direction of heat transfer (that is to say, assume the temperature of sewage water is higher than that of the pipe wall). Assume no thermal radiation occurs and omit thickness of the pipes, and then heat transfer in a REV can be written as Formula A-1.

$$q' = hA(t_s - t_i) \quad \text{(A-1)}$$

**q'**: *Heat flux of heat transfer per meters of sewage pipe in a REV, W/m*;

**h**: *Heat transfer coefficient, $W/m^2K$*;

**A**: *Surface area of the pipe contacting with sewage water per meter, $m^2/m$*;

**$t_s$**: *Temperature of sewage water, °C*;

**$t_i$**: *Temperature of the pipe wall in a REV, °C*

And total heat release of the REV is

$$Q_{REV} = q' L_{REV} \quad \text{(A-2)}$$

**$Q_{REV}$**: *Total heat release of the REV, W;*

**$L_{REV}$**: *Total sewage pipe length in a REV, m;*

Integrate $Q_{RVE}$ to derive total heat release of the study area, we can write that

$$Q_{SA} = \sum Q_{REV} = \sum (q' L_{REV}) = q' \sum L_{REV} = q' L_{SA} \quad \text{(A-3)}$$

Assume sewage pipes are distributing uniformly in Tokyo. Then there should be

$$\frac{L_{SA}}{S_{SA}} = \frac{L_{Tokyo}}{S_{Tokyo}} \quad \text{(A-4)}$$

**$L_{SA}$**: *Total sewage pipe length in the study area, m;*

**$S_{SA}$**: *Area of the study area, $km^2$;*

**$L_{Tokyo}$**: *Total sewage pipe length in Tokyo, m;*

**$S_{Tokyo}$**: *Area of Tokyo, $km^2$*

Consequently, $L_{SA} = S_{SA} \frac{L_{Tokyo}}{S_{Tokyo}}$ (A-5)

Then, $Q_{SA} = q' S_{SA} \frac{L_{Tokyo}}{S_{Tokyo}}$

(A-6)

Using 1884224 m, a total length of sewage pipes in Tokyo reported by the Sewage Statistics[47], $\frac{L_{Tokyo}}{S_{Tokyo}}$ can be calculated as 861.2 m/$km^2$.

$S_{SA}$ has been measured by Arc GIS as 6 $km^2$, so

$$Q_{SA} = 5.2 \times 10^3 q' = 5.2 \times 10^3 \, hA(t_s - t_i) \quad \text{(A-7)}$$

Values or treat of parameters in Formula A-7 are introduced below.

Correlation of h and flow velocity was reported by literature[30], as expressed in Formula A-8 and A-9.

$h=5.3+3.6v$ ($v \leqq 5$ m/s) (A-8)

$h=6.47v^{0.78}$ ($v > 5$ m/s) (A-9)

Even the fluid is sewage water in current study instead of air and textures of sewage pipes are not always concrete, since heat transfer in both the sewage pipe and the tunnel fall into one heat transfer mode (interphase transport in a nonisothermal system with a circular tube geometric feature[48]. Sewage pipes have been taken ideally as circular tubes), Formula A-8 and A-9 was thought somehow valid for an approximate calculation of h in heat transfer between the sewage water and the pipe wall. Use 1.8 m/s, the average value of designated maximum flow velocity and designated minimum flow velocity in a sewage pipe (calculated from the First Volume of Guideline for Planning and Designing Sewerage Facilities[47], h was calculated as 11.8 $W/m^2K$.

A was derived from an assumed average water depth in sewage pipes of the local sewage system. Spare room inside a sewage pipe is designated by the First Volume of Guideline for Planning and Designing Sewerage Facilities[47], as shown by Table A-1. Total length of the branch lines was thought to be much longer than that of the trunk line, thus the rule for pipes whose inner diameters are less than 700 mm (a pipe of this size range has been designated to be capable of draining a flow twice of the current draining demand) should be adopted. Ideally assume the cross sections of sewage pipes in the study area as circles, then it can be known that water depth inside a pipe should be half of the pipe diameter. Assume average radius of sewage pipes in the study area as 300 mm initially, then surface area of the pipe contacting with sewage water inside the pipe per meter is 0.9 $m^2/m$.

**Table A-1 Designated spare room in a sewage pipe** [47]

| Inner diameter of the pipe | Spare space |
|---|---|
| Under 700 mm | 100 % of the designated flow |
| Over 700 mm but under 1650 mm | Over 50 % but under 100 % of the designated flow |
| Over 1650 mm and under 3000 mm | Over 25 % but under 50 % of the designated flow |

A yearly temperature change of sewage water was reported by Kinouchi [49](Figure A-2), from year 1972 to year 2000, which was used to estimate $t_s$. However, for year 2001 to year 2017, the last time slot of the simulation duration, timely change of the sewage water temperature is unknown. Thus here infer the temperature change trend for this period using the monitor data taken by Kinouchi[49] (Figure A-2). The data have been explored by conducting regression analysis, and a significant linear correlation was found between the sewage water temperature and number of years from 1970, the starting year of the measurement (Figure A-3). Basing on the linear correlation, temperature of sewage water for year 2001-2017 was extrapolated.

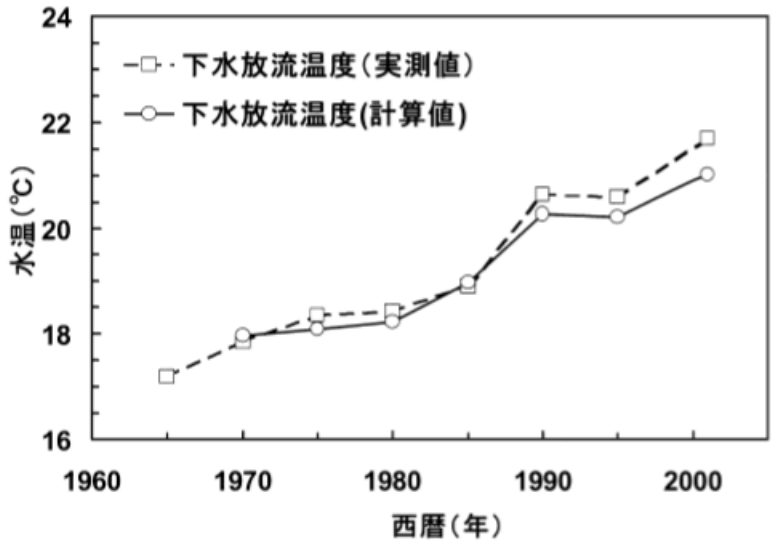


**Figure A-2 Monitored and simulated yearly temperature change of sewage water[49]**

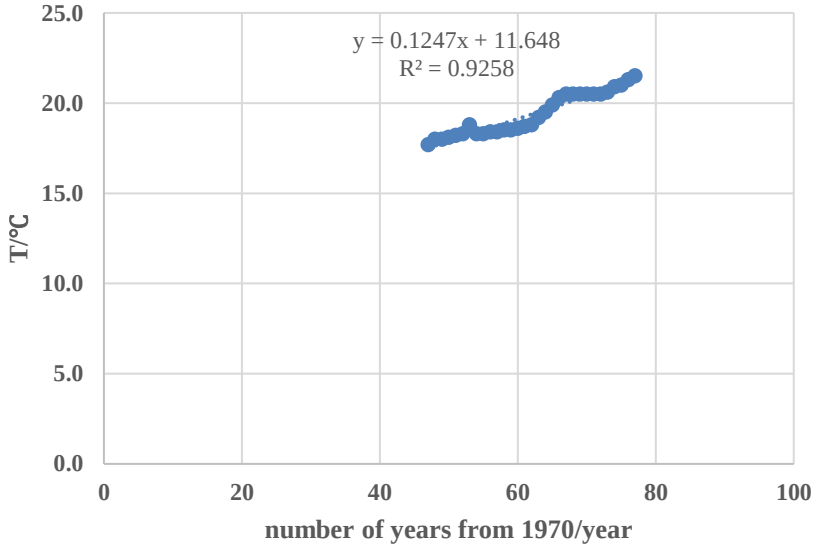


**Figure A-3 Linear correlation between sewage water and monitoring time**

.

At a scale as small as the REV, assume that the temperature of the pipe wall equals to the temperature in the strata. Consider the case when $\Delta x \rightarrow 0$, $\Delta y \rightarrow 0$ and $\Delta z \rightarrow 0$, then volume of the REV will endlessly approaching to 0, which means that temperature data at a model node in the FEFLOW model can be viewed as a representative for the average temperature in a REV, and consequently temperature in the strata surrounding that REV. Assume that the temperature of the pipe wall equals to the temperature of strata right beside the wall, in this way $t_i$ in Formula A-7 can be represented by temperature data at nodes in the FEFLOW model, which can be summoned in FEFLOW as an inner parameter when editing the sewage condition. The sewage heat source was planned to be given as a heat transfer boundary condition in FEFLOW software.

An average of the trunk line depth and the minimum soil covering thickness has been thought to be proper as an approximation for average depth of the plane heat source, because trunk lines of a sewage system can be much deeper than the average level of branch lines while a minimum soil covering thickness is always designated from secure perspective of view. Depth of the plane heat source was planned to be approximately given as 3 m beneath land surface.

## Reference


1. Taniguchi, M., Uemura, T. & Jago-on, K. Combined Effects of Urbanization and Global Warming on Subsurface Temperature in Four Asian Cities. *Vadose Zo. J.* **6,** 591 (2007).
2. Menberg, K., Bayer, P., Zosseder, K., Rumohr, S. & Blum, P. Subsurface urban heat islands in German cities. *Sci. Total Environ.* **442,** 123–133 (2013).
3. Ferguson, G. & Woodbury, A. D. Urban heat island in the subsurface. *Geophys. Res. Lett.* **34,** 2–5 (2007).
4. Lokoshchenko, M. A. & Korneva, I. A. Urban Climate Underground urban heat island below Moscow city. *URBAN Clim.* **13,** 1–13 (2015).
5. Müller, N., Kuttler, W. & Barlag, A. B. Analysis of the subsurface urban heat island in Oberhausen, Germany. *Clim. Res.* **58,** 247–256 (2014).
6. 西沢利栄. 熱汚染. (三省堂, 1977).
7. Fujii, K. Change in underground thermal environment due to human activity in urban area: with reference to the operation of subway lines. (The University of Tokyo, 2010).
8. Benz, S. A., Bayer, P., Menberg, K., Jung, S. & Blum, P. Spatial resolution of anthropogenic heat fluxes into urban aquifers. *Sci. Total Environ.* **524–525,** 427–439 (2015).
9. Gunawardhana, L. N. & Kazama, S. The potential role of urban green areas for controlling ground surface and subsurface warming. *Urban Water J.* **9006,** 1–11 (2015).
10. Luo, Z. & Asproudi, C. Subsurface urban heat island and its effects on horizontal ground-source heat pump potential under climate change. *Appl. Therm. Eng.* **90,** 530–537 (2015).
11. Zhu, K., Blum, P., Ferguson, G., Balke, K. & Bayer, P. The geothermal potential of urban heat islands. *Environ. Res. Lett.* **5,** 44002 (2010).
12. 東京都下水道局. 第 8 章 東京下水道の歴史.
13. 東急電鉄. 各路線概要. Available at: http://www.tokyu.co.jp/railway/data/train_line/.
14. 東京メトロ. 沿革. Available at: http://www.tokyometro.jp/corporate/profile/history/index.html.
15. 首都高速道路株式会社. 中央環状線 山手トンネル. Available at: http://www.shutoko.jp/ss/tokyo-smooth/shinagawa/tunnel/.
16. 国土交通省. 5万分の1都道府県土地分類基本調査（東京西南部）. Available at: http://nrb-www.mlit.go.jp/kokjo/inspect/landclassification/land/5-1/1308.html.
17. 国土地理院. 平面直角座標系（平成十四年国土交通省告示第九号）. Available at: http://www.gsi.go.jp/LAW/heimencho.html.
18. 日本地下水学会. 都内湧き水めぐり. Available at: http://www.jagh.jp/content/shimin/images/wakimizu/20111002/kaisetsu.pdf.
19. 気象庁. 過去の気象データ検索. Available at: http://www.data.jma.go.jp/obd/stats/etrn/index.php?sess=6ef525a9cdef28cea634ce58ca736e68.
20. 日本地下水学会. 降雨による地下水涵養量は年間でどのくらいあるの？. Available at: http://www.jagh.jp/jp/g/activities/torikichi/faq/5.html.
21. 東京都水防災総合情報システム. 水位グラフ 目黒川. Available at: http://www.kasen-suibo.metro.tokyo.jp/im/uryosuii/tsim0106g_2B16.html.
22. 東京都水防災総合情報システム. 水位グラフ 渋谷川. Available at: http://www.kasen-suibo.metro.tokyo.jp/im/uryosuii/tsim0106g_2B12.html.

23. 東京都建設局. 地質断面図の選択. Available at: http://www.kensetsu.metro.tokyo.jp/jigyo/tech/start/03-jyouhou/danmenzu/danmenzu.html.
24. 新藤 静夫. 武蔵野台地の水文地質. 地学雑誌 **77,** 223–246 (1968).
25. 島野安雄 & 藪崎志穂. 東京都心部における湧水・井戸水などの地下水の水質特性. *文星紀要 = Bunsei Bull.* 103–136 (2015).
26. 東京都土木技術研究所. 浅層地下水位年表 - 東京都地質図集 5 一. (1991).
27. 藤縄克之. 環境地下水学. (共立出版, 2010).
28. 国土地理院. 土地利用の変遷. (1984). Available at: http://www.gsi.go.jp/atlas/archive/j-atlas-kokudo-d_j_06.pdf.
29. 津守澄男, 永持理 & 関高. 東急東横線渋谷駅～代官山駅間地下化工事の概要. 地下空間シンポジウム論文・報告集 **14,** 251–256 (2009).
30. 坂本 誠, 武田 仁 & 矢崎 淳史. 4238 地下鉄の排熱に関する基礎的調査 : その1 調査概要と実測データ. *学術講演梗概集. D, 環境工学* **1993,** 475–476 (1993).
31. 矢崎巧. 首都高速中央環状線山手トンネル内の温度上昇抑制対策の概要. 地下空間シンポジウム論文・報告集 **20,** 213–220 (2015).
32. 三浦 昌生 & 尾島 俊雄. 東京における地中温度分布に関する実測調査研究. 日本建築学会計画系論文報告集 11–18 (1985).
33. 東修三. 気温と地表面温度の年平均値の差異に対する熱平衡論的考察. in (日本気象学会総会, 1951).
34. 鈴木 宏芳. 関東平野の地中温度. *国立防災科学技術センタ-研究報告* p139-154 (1985).
35. 玄地 裕 *et al.* 都市ヒートアイランド現象が地温に与える影響 : 東京都内における観測結果. 天気 **45,** 707–715 (1998).
36. Google. Google map. Available at: https://www.google.co.jp/maps/@35.6518919,139.6892781,286m/data=!3m1!1e3.
37. 武田 仁. 地下鉄の排熱利用のための温熱環境実測調査. 日本建築学会計画系論文集 7–15 (1995).
38. 東京の南西部、狛江市から北東端となる葛飾区にかけての地層分布を示した模式断面図. Available at: http://www.tokyo-geo.com/tikei/tishitu1.htm.
39. 国土交通省国土政策局国土情報課. 国土数値情報ダウンロードサービス. Available at: http://nlftp.mlit.go.jp/ksj/.
40. 今尾恵介. 地下鉄 縦断面図. 日本鉄道旅行地図帳・東京 6~7 (2008).
41. 東京急行電鉄株式会社. 新玉川線建設史. (東京急行電鉄, 1980).
42. 寺島善宏. 各論：地質および構造の概要. 基礎工 **43,** 18~21 (2013).
43. 菅原 広史 & 近藤 純正. 都市における各種地表面温度の敏感度解析. 天気 **42,** 813–818 (1995).
44. 東京都. 目黒川流域河川整備基本方針. (2014).
45. 谷謙二. 今昔マップ on the web. Available at: http://ktgis.net/kjmapw/kjmapw.html?lat=35.681287&lng=139.76323100000002&zoom=14&dataset=tokyo50&age=0&map2type=roadmap&dual=true.
46. 東京都下水道局. みんなの下水道 - 地図で探そう. Available at: http://www.gesui.metro.tokyo.jp/kids/minna/map/meguro.htm.
47. 日本下水道協会. 下水道統計. (日本下水道協会, 2013).
48. Bird, R Byron and Stewart, Warren E and Lightfoot, E. N. *Transport phenomena*. (1960).
49. 木内 豪. 都市の水・エネルギー利用が水域に及ぼす熱影響のモデル化と東京都区部下

水道への適用. 水文・水資源学会誌 **17,** 13–21 (2004).